Les Cahiers du GERAD ISSN: 0711–2440

Two decomposition algorithms for solving a minimum weight maximum clique model for the air conflict resolution problem

T. Lehouillier, J. Omer,
F. Soumis, G. Desaulniers

G–2015–103

October 2015

GERAD HEC Montréal
3000, chemin de la Côte-Sainte-Catherine
Montréal (Québec) Canada H3T 2A7

Tél. : 514 340-6053
Téléc. : 514 340-5665
info@gerad.ca
www.gerad.ca

Two decomposition algorithms for solving a minimum weight maximum clique model for the air conflict resolution problem

Thibault Lehouillier
Jérémy Omer
François Soumis
Guy Desaulniers

GERAD & Polytechnique Montréal, Montréal (Québec) Canada, H3C 3A7

thibault.lehouillier@gerad.ca
jeremy.omer@gerad.ca
francois.soumis@gerad.ca
guy.desaulniers@gerad.ca

October 2015

Les Cahiers du GERAD
G–2015–103

Abstract: In this article, we tackle the conflict resolution problem using a new variant of the minimum weight maximum clique model. The problem consists in identifying maneuvers that maintain the required separation distance between all pairs of a set of aircraft while minimizing fuel costs. To this end, we design a graph whose vertices correspond to a finite set of maneuvers and whose edges connect conflict-free maneuvers. A maximum clique of minimal weight yields a conflict-free situation involving all aircraft and minimizing the costs induced. The innovation of the model relies on the cost structure: the cost of the vertices cannot be determined a priori, since they depend on the vertices in the clique. To tackle this feature, we formulate the problem as a mixed integer linear program. Since the modeling of aircraft dynamics and the computation of trajectories is separated from the solution process, the model is flexible. As a consequence, the mathematical framework presented in this article remains valid, whatever the hypotheses considered. In particular, in this paper aircraft can perform dynamic velocity, heading and flight level changes. To solve instances involving a large number of aircraft spread on several flight levels, we introduce two decomposition algorithms: the first one is a sequential mixed integer linear optimization procedure that iteratively refines the discretization of the maneuvers to yield a trade-off between solution time and cost. The second is a large neighborhood search heuristic that uses the first one as a subroutine. The best solutions for the available set of maneuvers are obtained in less than 10 seconds for instances with up to 250 aircraft randomly allocated to 20 flight levels.

Key Words: Air traffic control, conflict resolution, mixed integer linear optimization, graph theory, decomposition methods.

Résumé : Nous présentons un modèle déterministe pour le problème de détection et de résolution de conflits entre aéronefs. Les aspects liés à la dynamique des avions, à leurs manœuvres ainsi que la fonction de coûts sont complètement séparés du processus de résolution. En conséquence, le formalisme mathématique présenté reste valide, et ce quelles que soient les hypothèses faites sur les avions, les manœuvres et les coûts. Nous modélisons le problème comme une recherche de clique de cardinalité maximale et de coût minimum dans un graphe. Les sommets du graphe correspondent à des manœuvres des aéronefs, et les arêtes connectent des manœuvres sans conflit d'aéronefs distincts. Ce modèle est en fait une nouvelle variante du problème de recherche de clique de coût minimum, dans le sens où les coûts des sommets dépendent des sommets de la clique. Nous formulons cette nouvelle variante comme un programme linéaire à variables mixtes. Nous présentons également deux méthodes de décomposition pour le problème. La première vise à étudier l'impact du nombre de manœuvres par aéronef sur le temps de résolution, et permet de trouver un compromis entre effort calculatoire et efficacité de la solution. La seconde vise à exploiter la structure géométrique de l'ensemble d'aéronefs considérés. Des instances ayant jusque 65 avions sur un seul niveau sont résolues en moins de deux minutes par le modèle classique, et les méthodes de décomposition permettent de résoudre des instances ayant jusque 250 avions répartis sur 20 niveaux de vol en moins de 10 secondes.

Acknowledgments: This work was carried out under the project OPR-601 funded by the CRIAQ (Consortium on Research and Innovation in Aerospace in Quebec).

1 Introduction

1.1 Context: Challenges of air traffic control

In the last few years air traffic management (ATM) has attracted more and more attention, in particular with research on advanced decision algorithms. Such automated tools are recognized as key-components of future ATM systems like the Single European Sky ATM Research (SESAR) [1] project in Europe and the Next Gen [2] program in the United States. Optimization algorithms for air traffic control (ATC) are particularly relevant in the current context of growing traffic, where the airspace capacity and safety become issues. Indeed, the latest long-term forecast published by EUROCONTROL states that the traffic demand will increase by 20% to 80% between 2012 and 2035 [3]. Besides, a simulation-based study performed by Lehouillier et al. [4] shows that for a 50% increase in traffic, the controllers in charge of busy sectors would have to solve on average 27 conflicts per hour. This workload exceeds the human capacity and decision tools are necessary to help the controllers.

1.2 Literature review

One complex and central problem encountered in ATC is the air conflict resolution (CR) problem. A conflict occurs when two aircraft are too close to each other regarding predefined horizontal and vertical separation distances of respectively 5NM and 1000ft, as illustrated in Figure 1. To resolve a conflict, the controllers issue maneuvers that can be either speed, heading or altitude changes. Given the current position, speed, acceleration and the predicted trajectory of a set of aircraft, the CR problem consists in identifying the conflict-free maneuvers that minimize a given cost function. The CR problem is one of the most widely studied problems in ATM. We provide a synthetic analysis of the studies that were most influential to our work, but a more complete coverage of the existing literature may be found in the review performed in Martìn-Campo's thesis [5]. Because aircraft trajectories are time-continuous, the most natural approach is to model the problem with optimal control [6]. Analytical solutions can be found only for the simplest cases, but coupled with nonlinear programming techniques, the models can be solved numerically. For instance, Raghunathan et al. [7] use a time discretization of the problem to derive solutions for instances with more than two aircraft. One difficulty is that the nonlinear program (NLP) is nonconvex, so the global optimum cannot be found in a reasonable amount of time and the solution is very sensitive to the starting point.

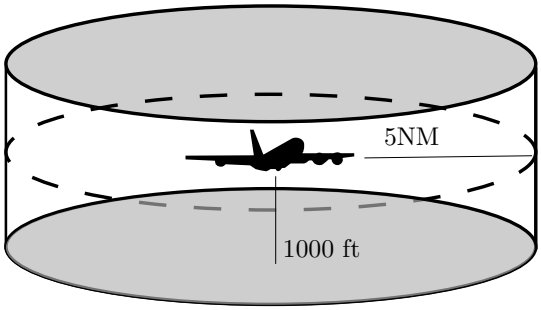

Figure 1: Safety cylinder around an aircraft

To find feasible solutions in a few seconds, several heuristics have been developed. Durand and Alliot [8] and Meng and Qi [9] develop an ant colony algorithm, where maneuvers are chosen within a finite discrete set of heading changes performed at constant speed. Alonso-Ayuso et al. [10] adapt a variable neighborhood search algorithm considering only heading changes. Other fast methods include conflict resolution using maneuvers extracted from a prescribed set [11], particle swarm optimization (see Gao et al. [12] for heading changes), or neural networks (see Durand et al. [13], Christodoulou and Kontegeorgous [14] for speed changes). Such methods present the asset of bringing fast solutions, but the convergence is not guaranteed.

Mixed integer linear and nonlinear programming are powerful theoretical frameworks for the study of CR. With the realistic restriction that the aircraft perform at most one maneuver at the initial time, Pallot-

tino et al. [15] exploit the geometry of the separation constraints to develop two mixed integer linear programs (MILPs) that allow either a speed change with constant heading or a heading change with constant speed. In the same context, Vela et al. [16] develop a MILP that considers both speed and heading changes, and Christodoulou and Costoulakis [17] describe a nonlinear model for three-dimensional conflict resolution. Another MILP has been described by Alonso-Ayuso et al. [18] to allow both velocity and altitude changes. In [19], Alonso-Ayuso et al. also extend the model of [15] by introducing continuous instead of instantaneous speed changes. Schouwenaars [20] or, more recently, Omer and Farges [21] perform a time-based discretization of the optimal control formulation. Vela et al. [**?**] and Omer [22] also develop MILPs with a space discretization that focus on the main points of interest of the conflict resolution.

Graph theory has also been used in ATM, but mostly for air traffic flow management (ATFM) [23, 24]. In ATC, conflicts between aircraft are generally modeled by a graph whose vertices represent the different aircraft and whose edges link pairs of conflicting aircraft. Vela [25] and Sherali et al. [26] use conflict graphs in their models. Resmerita et al. [27] study *a priori* conflict resolution by developing a multi-agent system where each aircraft has to choose a path in a resource graph whose vertices represent zones of the airspace and where chosen paths have to be conflict-free. Barnier and Brisset [28] assign different flight levels to aircraft with intersecting routes by looking for maximum cliques in a graph defining an assignment of all aircraft to a set of given flight levels.

1.3 Contribution statement

In this paper, we present a formulation of the CR problem as a variant of the minimum-weight and maximum cardinality clique (MWMCC) problem. We design a graph whose vertices represent possible aircraft maneuvers and where edges link conflict-free maneuvers of different aircraft. The innovation of this model relies on the cost structure. Indeed, the costs of the vertices are not known *a priori* since they depend on which maneuvers are in the clique. This model is flexible because it separates the resolution process from the modeling of the aircraft dynamics and their maneuvers. As a consequence, the mathematical framework used in the optimization method remains valid whatever the considered hypotheses on the aircraft dynamics and maneuvers, the computation of separation distances and the cost evaluation method. This feature highlights robustness, which is really important in ATC because we want to solve a large span of conflicts. For a fast solution of large instances, the explosion of the number of vertices needs to be addressed, since it is critical in terms of computational effort. To this end, we develop two decomposition algorithms. The first one is a sequential mixed integer linear optimization (SMILO) procedure that iteratively refines the discretization of the set of maneuvers without changing the number of vertices in the graph. This yields a trade-off between solution time and the cost of the optimal solution. This procedure is then used as a subroutine within a spatial decomposition that takes advantage of the geometric structure of the instances. The spatial decomposition is a large neighborhood search metaheuristic exploiting the weak interdependency between subsets of aircraft.

Finally, we test our model on an extended benchmark that includes structured instances with up to 20 aircraft, and random instances involving up to 60 aircraft on a single flight level and 250 aircraft on several flight levels. From a practical point of view, the results show that automated conflict resolution could be performed for large and dense areas of the airspace within a few seconds.

2 Problem formulation

In this section, we detail the modeling of the aircraft dynamics and maneuvers, the computation of separation distances and the cost evaluation method. The choices or assumptions made in this section represent a possible modeling of the problem. Nevertheless, since they are fully independent of the resolution method, considering other alternatives would not impact the validity of the overall method presented in this article.

2.1 Modeling aircraft dynamics

As in the majority of the literature, we use a three-dimensional point-mass model for aircraft dynamics:

$$\frac{dp_x}{dt} = V\cos\gamma\cos\chi \quad (1)$$
$$\frac{dp_y}{dt} = V\cos\gamma\sin\chi \quad (2)$$
$$\frac{dp_z}{dt} = V\sin\gamma \quad (3)$$
$$\frac{d\gamma}{dt} = \frac{g_0}{V}(n\cos\phi - \cos\gamma) \quad (4)$$
$$\frac{d\chi}{dt} = \frac{g_0}{V}\frac{n\sin\phi}{\cos\gamma} \quad (5)$$
$$\frac{dV}{dt} = \frac{F_T - F_D}{m} - g_0\sin\gamma \quad (6)$$

The position of the aircraft is given by the coordinates (p_x, p_y, p_z) of its center of gravity in a local coordinate system, (p_x,p_y) being its coordinates in a horizontal plane and p_z its altitude. The aircraft flies at speed V and the angles χ, ϕ and γ correspond respectively to its heading, roll and pitch. Variables F_T and F_D denote the norm of the thrust and drag forces respectively, m is the aircraft mass, n is the load factor and g_0 corresponds to the gravitational acceleration.

We assume that aircraft follow their trajectory with a stepwise constant acceleration. Maneuvers are executed with a constant acceleration and yaw rate, and the speed vector remains constant between two consecutive maneuvers. This assumption is realistic because it respects the time-continuity of speed, and it corresponds to a setting where maneuvers are performed smoothly. If other speed changes were to be considered, it would not jeopardize the resolution process, since it will solely impact the computation of the separation distances and maneuvers costs.

In the remainder of the article, $\mathcal{F} = [\![1; N]\!]$ denotes the set of the considered aircraft.

2.2 Aircraft maneuvers

2.2.1 Types of maneuvers

The maneuvers considered can be of the following types:

- variable *NIL* refers to the *null* maneuver, i.e., when no maneuver is performed;
- variable H_θ is a heading change by an angle $\theta \in [-\pi; \pi]$[1];
- variable S_δ is a relative speed change of δ%. We use relative speed changes because they have already been chosen in large-scale projects such as ERASMUS [29];
- variable $V_{\delta h}$ is a change of δh flight levels.

Figure 2 describes the geometry of the heading change and the flight level change. Heading changes are performed in a turning point fashion as depicted on Figure 2a. Flight level changes are followed by a return toward the initial flight level, as on Figure 2b.

We define $\mathcal{M} = \cup_{f=1}^{n}\mathcal{M}_f$ as the set of all possible maneuvers, $\mathcal{M}_f$ being the set of maneuvers for aircraft $f \in \mathcal{F}$.

2.2.2 Dynamics of the maneuvers

Since the analysis carried out by Omer [21] concludes that considering instantaneous maneuvers can lead to a significant error in the separation distance, we follow the model with constant acceleration described

[1] positive angles correspond to counter-clockwise rotations

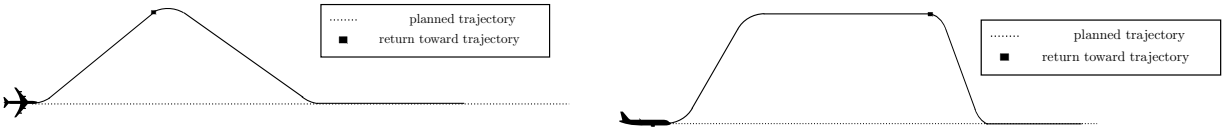

(a) Projection of a heading change on the horizontal plane

(b) Projection of a flight level change on a vertical plane

Figure 2: Geometry of the heading change and the flight level change

in [30]. In [30], Paielli states that the typical acceleration during a speed adjustment for commercial transport aircraft is in the order of 0.4kn/s or 0.02 g. This value is set to respect the comfort of passengers. Heading changes are approximated by a steady turn of constant rate and radius, given by the following equations:

$$\omega = \frac{d\chi}{dt} = \frac{g_0 \tan\phi}{V} \tag{7}$$

$$r = \frac{V^2}{g_0 \tan\phi} \tag{8}$$

We also consider the altitude maneuvers to be dynamic. The changes of flight level are performed with a vertical speed which is a function of thrust, drag, and true airspeed. Details on the computation of the vertical speed can be found in the BADA user manual [31].

2.2.3 Trajectory recovery

In this article, we consider that aircraft follow a 4D contractual trajectory, which represents a compromise between the user's preferences and the capacity constraints of the network. The trajectories of the aircraft then have to meet time and space requirements over a sequence of 4D points. Noncompliance with this contract induces penalty fees to companies. As a consequence, it is important to make sure that, after resolving every conflict, every aircraft recovers its initial 4D trajectory. Ensuring a strict velocity control can be very costly and almost impossible in practice. Time recovery is therefore not required, but it is favored by giving a penalty on the time shift between the trajectory without conflict and the 4D trajectory after the loss of separation is avoided. The method for computing the penalty costs follows the one by Omer [21]: the penalty shift is estimated as the total cost induced by a time recovery of the 4D trajectory, at a speed depending on the sign of the shift.

2.2.4 Maneuvers costs

In this subsection we give some details about the computation of the cost of a maneuver. The purpose is to highlight that, even though computations can be complex, it does not interfere whatsoever with the resolution method that is described in Section 4. Additionally, if more complex cost models were to be considered, it would be possible without changing anything in the solution method.

For a jet commercial aircraft f with constant altitude, the fuel consumption by time and distance unit is given by (9) and (10):

$$C_{t,f}\left(t, V_f(t)\right) = c_{1,f}\left(1 + \frac{V_f(t)}{c_{2,f}}\right) F_{T,f}(t) \tag{9}$$

$$C_{d,f}\left(t, V_f(t)\right) = \frac{C_{t,f}\left(t, V_f(t)\right)}{V_f(t)} \tag{10}$$

where variables $c_{1,f}$ and $c_{2,f}$ are numerical constants depending on the type of aircraft f.

Depending on the type of the maneuver, a different approach is followed.

Speed change. Consider a change of speed $V_f' = V_f^n(1+\delta)$ during a time t, where variable V_f^n is the nominal speed of aircraft f. Let C_{speed} denote the cost of the maneuver. Variable C_{speed} is the sum of:

1. the cost of the additional fuel burnt during the maneuver, C_s^f;
2. the penalty for not respecting the 4D contract, C_s^{4D}.

$$C_{\text{speed}} = C_s^f + C_s^{4D} \tag{11}$$

To compute C_s^f, it is useful to distinguish the cost incurred during the the transition from V_f^n to V_f', C_s^t, and that incurred on the portion of trajectory flown with the new speed, C_s^n:

$$C_s^f = C_s^t + C_s^n \tag{12}$$

Let $t_{\delta,V}$ denote the time required to go from V_f^n to V_f'. We compute C_s^t as the following expression

$$C_s^t = \int_0^{t_{\delta,V}} C_{t,f}\left(t, V_f(t)\right) dt - t_{\delta,V} C_{t,f}\left(t, V_f^n\right) \tag{13}$$

The cost C_s^n is given by

$$C_s^n = (t - t_{\delta,V})\left(C_{t,f}(t, V_f') - C_{t,f}(t, V_f^n)\right) \tag{14}$$

The penalty C_s^{4D} is deduced from the delay d_s^{4D} created by the maneuver, which is computed as follows.

$$d_s^{4D} = \int_0^{t_{\delta,V}} V_f(t)dt + (t - t_{\delta,V})V_f' - tV_f^n \tag{15}$$

Depending on the sign of d_s^{4D}, a different recovery speed is used to catch up with the 4D trajectory, inducing the cost C_s^{4D}.

Heading change. Let C_{heading} denote the cost of a heading change by an angle θ during a period t. The quantity C_{heading} is decomposed as the sum of:

1. the cost on the additional distance induced by the maneuver, C_h^d;
2. the penalty for not respecting the 4D contract, C_h^{4D}.

$$C_{\text{heading}} = C_h^d + C_h^{4D} \tag{16}$$

To recover the spatial trajectory, the aircraft performs a turn with an angle -2θ as detailed on Figure 3.

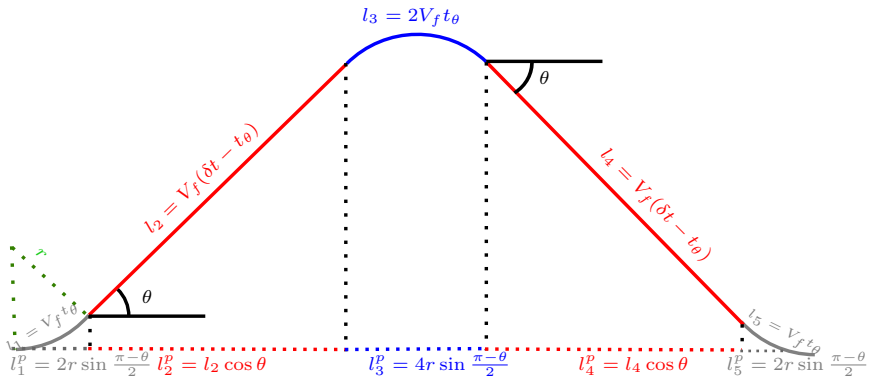

Figure 3: Geometry of the trajectory recovery following a heading change

The aircraft flies an extra distance d given by

$$d = \sum_{i=1}^{5} l_i - l_i^p \tag{17}$$

where the expressions of the variables l_i and l_i^p are given on Figure 3. The cost of the extra fuel burnt on d is then computed as follows:

$$C_d^h = C_{d,f}(t, V_f)d \tag{18}$$

The penalty C_h^{4D} is then deduced from the delay d_h^{4D} due to the extra distance, d, flown during the heading change:

$$d_h^{4D} = \frac{d}{V_f^n} \tag{19}$$

where d is the extra distance flown during the maneuver. Depending on the sign of d_h^{4D}, a different recovery speed is used to catch up with the 4D trajectory, inducing the cost C_h^{4D}.

Flight level change. Consider a change of δh flight levels during a period t. To illustrate the geometry of the maneuver, Figure 4 details the example where an aicraft climbs one level.

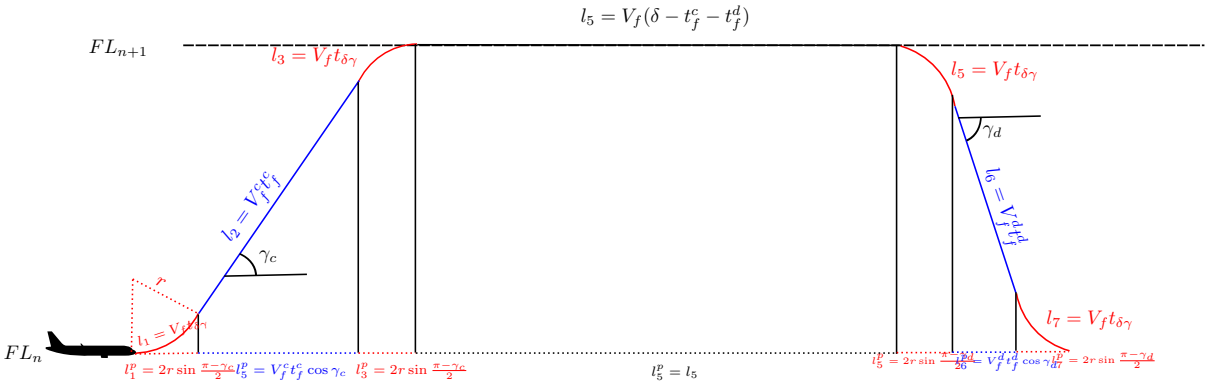

Figure 4: Geometry of the trajectory recovery following a flight level change

Let C_{FL} denote the cost of this maneuver. Variable C_{FL} is the sum of the following quantities:

1. the extra cost during the ascent and descent, denoted C_{FL}^a and C_{FL}^d, respectively;
2. the difference between the cost on the initial flight level and that on the new flight level, denoted $C_{\text{FL}}^{\delta h}$;
3. the cost on the additional distance flown d denoted C_{FL}^d;
4. the 4D contract penalty C_{FL}^{4D}.

$$C_{\text{FL}} = C_{\text{FL}}^a + C_{\text{FL}}^d + C_{\text{FL}}^{\delta h} + C_{\text{FL}}^d + C_{\text{FL}}^p \tag{20}$$

C_{FL}^a and C_{FL}^d are derived by

$$C_{\text{FL}}^a = t_a \left(C_{a,t}(f, V_f^a) - C_{t,f}(t, V_f^n) \right) \tag{21}$$

$$C_{\text{FL}}^d = t_d \left(C_{d,t}(f, V_f^d) - C_{t,f}(t, V_f^n) \right) \tag{22}$$

where t_a , t_d are the durations of ascent and descent, $C_{a,t}$ and $C_{d,t}$ are the fuel costs during the climb and the descent, and V_f^a and V_f^d represent the climb and descent speeds, respectively. The fuel consumption and the ascent and descent speeds are taken from the BADA tables corresponding to the aircraft types.

Equation (23) derives the difference of fuel consumption between the two levels.

$$C_{\text{FL}}^{\delta h} = (\delta t - t_a - t_d)(C_{FL_{n+\delta h}} - C_{FL_n}) \tag{23}$$

where $C_{FL_{n+\delta h}}$ and C_{FL_n} denote the fuel consumption per time unit on the new and initial flight level, respectively. The fuel burnt on the additional distance flown d is derived with (24).

$$C^d_{\mathrm{FL}} = C_{d,f}(t, V_f)d \tag{24}$$

where the distance d is computed by (25):

$$d = \sum_{i=1}^{7} l_i - l_i^p \tag{25}$$

where the expressions of the variables l_i and l_i^p are given on Figure 4.

The computation of the 4D contract penalty, C^{4D}_{FL}, is then similar to that performed for the heading maneuvers.

2.3 Aircraft separation

To determine whether two aircraft are separated we use the following notation:

- $\mathcal{T}$: time horizon for the conflict resolution;
- $\boldsymbol{p}_i(t) \in \mathbb{R}^3$: position vector of aircraft i at time t. Variables $p_{i,x}(t)$ $p_{i,y}(t)$ and $p_{i,z}(t)$ denote respectively the abscissa, ordinate and altitude components of the position vector;
- $\boldsymbol{s}_i(t) \in \mathbb{R}^3$: speed vector of aircraft i at time t. Variables $s_{i,x}(t)$ $s_{i,y}(t)$ and $s_{i,z}(t)$ denote respectively the abscissa, ordinate and altitude components of the speed vector;
- $\boldsymbol{a}_i(t) \in \mathbb{R}^3$: acceleration vector of aircraft i at time t. Variables $a_{i,x}(t)$ $a_{i,y}(t)$ and $a_{i,z}(t)$ denote respectively the abscissa, ordinate and altitude components of the acceleration vector.

Let i and j be two aircraft applying maneuvers m_i and m_j, respectively. Aircraft i and j are said to be separated at time t if and only if at least one of constraints (26) and (27) holds.

$$d^h_{ij}(t)^2 = (p_{i,x}(t) - p_{j,x}(t))^2 + (p_{i,y}(t) - p_{j,y}(t))^2 \geq D^2_{\mathrm{h,min}} \tag{26}$$
$$d^v_{ij}(t)^2 = (p_{i,z}(t) - p_{j,z}(t))^2 \geq D^2_{\mathrm{v,min}} \tag{27}$$

At any time $t \in \mathcal{T}$, either none, one or both aircraft are maneuvering. The set $\mathcal{T}$ can thus be divided into intervals where both i and j have a constant acceleration. For each interval, we compute the time at which the aircraft are the closest to verify if the separation constraints hold. Let $\mathcal{T}_k$ be one of these intervals. Consider i and let $t_0 \in \mathcal{T}$ be the starting time of maneuver m_i. If we assume that maneuver m_i is applied with a constant acceleration, we obtain the position and the speed vector of i at time $t_0 + t$ with t such that $t - t_0 \leq |\mathcal{T}_k|$:

$$\boldsymbol{p}_i(t_0 + t) = \boldsymbol{p}_i(t_0) + (t - t_0)\boldsymbol{s}_i(t_0) + \frac{(t - t_0)^2}{2}\boldsymbol{a}_i(t_0) \tag{28}$$
$$\boldsymbol{s}_i(t_0 + t) = \boldsymbol{s}_i(t_0) + (t - t_0)\boldsymbol{a}_i(t_0) \tag{29}$$

Let $\boldsymbol{p}^h_{ij}$ (respectively $\boldsymbol{s}^h_{ij}$, $\boldsymbol{a}^h_{ij}$) denote the horizontal position (respectively the speed and the acceleration) of aircraft j relatively to aircraft i. We define

$$\begin{aligned} d^h_{ij}(t + \tau) &= ||\boldsymbol{p}^h_{ij}(t + \tau)|| \\ &= ||\boldsymbol{p}^h_{ij}(t) + \tau \boldsymbol{s}^h_{ij}(t) + \frac{\tau^2}{2}\boldsymbol{a}^h_{ij}(t)|| \end{aligned}$$

where $\tau \geq 0$.

Let $\tau_{ij} \in \underset{\tau \geq 0}{\operatorname{argmin}} d^h_{ij}(t + \tau)^2$, and $t^h_{ij} \in \underset{t \in \mathcal{T}}{\operatorname{argmin}} d^h_{ij}(t)^2$.

We have:

$$t_{ij}^h = \begin{cases} 0 & \text{if } \tau_{ij} = 0 \\ |\mathcal{T}_k| & \text{if } \tau_{ij} \geq |\mathcal{T}_k| \\ \tau_{ij} & \text{otherwise} \end{cases}$$

where $|\mathcal{T}_k|$ is the length of interval $\mathcal{T}_k$. Aircraft i and j are horizontally separated during interval $\mathcal{T}$ if and only if

$$d_{ij}^h (t_{ij}^h)^2 \geq D_{\text{h,min}}^2 \tag{30}$$

By a similar reasoning, aircraft i and j are vertically separated during interval $\mathcal{T}$ if and only if

$$d_{ij}^v (t_{ij}^v)^2 \geq D_{\text{v,min}}^2 \tag{31}$$

Let $\mathcal{I}_{i,j}^h$ and $\mathcal{I}_{i,j}^v$ denote the intervals during which i and j are not separated horizontally and vertically, respectively. i and j are separated if and only if

$$\mathcal{I}_{i,j}^h \cap \mathcal{I}_{i,j}^v = \emptyset \tag{32}$$

3 Modeling the CR problem as a MWMCC problem

In this section, we describe how the CR problem can be modeled as a MWMCC problem. This model is based on a preliminary study that we presented in [32].

3.1 Graph theory definitions

Let $\mathcal{G} = (\mathcal{V}, \mathcal{E})$ be an undirected, simple graph with a vertex set $\mathcal{V}$ and an edge set $\mathcal{E} \subseteq \mathcal{V} \times \mathcal{V}$.

A *clique* in graph $\mathcal{G}$ is a vertex set $\mathcal{C}$ with the property that each pair of vertices in $\mathcal{C}$ is linked by an edge:

$$\mathcal{C} \subseteq \mathcal{V} \text{ is a clique} \Leftrightarrow \forall (u, v) \in \mathcal{C} \times \mathcal{C}, u \neq v, (u, v) \in \mathcal{E} \tag{33}$$

A *maximum* clique in $\mathcal{G}$ is a clique that is not a subset of any other clique in $\mathcal{G}$. The cardinality of a maximum clique of $\mathcal{G}$ is called *clique number* and is denoted by $w(\mathcal{G})$. Let $c : \mathcal{V} \to \mathbb{R}$ be a vertex-weight function associated with $\mathcal{G}$. A *maximum* clique of *minimum* weight in $\mathcal{G}$ is a maximum clique $\mathcal{C}$ that minimizes $\sum_{v \in \mathcal{C}} c(v)$.

A *stable set* $\mathcal{S} \subseteq \mathcal{V}$ is a subset of vertices no two of which are adjacent in $\mathcal{G}$. A *bipartite* graph is a graph whose vertices can be partitioned into two distinct stable sets $\mathcal{V}_1$ and $\mathcal{V}_2$. Each edge of the graph then connects one vertex of $\mathcal{V}_1$ to a vertex of $\mathcal{V}_2$. This concept is extended to $k-$*partite* graphs, where the vertex set is partitioned into k distinct stable sets.

The *density* of a graph $\mathcal{G} = (\mathcal{V}, \mathcal{E})$ is defined as the ratio of the number of edges $|\mathcal{E}|$ over the number of edges in a complete graph with $|\mathcal{V}|$ vertices:

$$d_{\mathcal{G}} = \frac{|\mathcal{E}|}{\frac{|\mathcal{V}|(|\mathcal{V}|-1)}{2}} \tag{34}$$

3.2 Graph construction

In this subsection, we introduce the *conflict graph* $\mathcal{G} = (\mathcal{V}, \mathcal{E})$ used to model the CR problem.

3.2.1 Defining the vertices

The set of vertices is defined as $\mathcal{V} = [\![1; |\mathcal{M}|]\!]$. We note $\mathcal{V}_f$ the set of vertices corresponding to aircraft f. In emergency scenarios where the feasibility of the problem can be an issue, it is possible to introduce n vertices corresponding to costly emergency maneuvers. Such maneuvers have already been studied, and can for instance correspond to maneuvers implemented by the Terminal Collision Avoidance system [33], or to the maneuvers described by Schouwenaars [20]. However, since feasibility has not been an issue in our tests, we did not add these vertices in our implementation.

3.2.2 Defining the edges

Let $(i, j) \in \mathcal{V} \times \mathcal{V}$ be a pair of vertices representing maneuvers $(m_i, m_j) \in \mathcal{M} \times \mathcal{M}$ of aircraft $(i, j) \in \mathcal{F} \times \mathcal{F}$. For $i \neq j$, we write $m_i \square m_j$ when no conflict occurs if aircraft i follows maneuver m_i while aircraft j performs maneuver m_j. The set of edges $\mathcal{E}$ corresponds to the pairs of maneuvers performed by two different aircraft without creating conflicts:

$$\mathcal{E} = \{(i, j) \in \mathcal{V} \times \mathcal{V}, i \neq j : m_i \square m_j\} \tag{35}$$

3.2.3 Relative density

We can define a measure of density taking advantage of the structure of the conflict graph. Indeed, it is important to note that there is no edge between two different maneuvers of a given aircraft, which yields Observation 3.1.

Observation 3.1 *For all $f \in \mathcal{F}, \mathcal{V}_f$ is a stable set, i.e there is no edge linking two distinct vertices of $\mathcal{V}_f$. Hence, the graph $\mathcal{G}$ is $|\mathcal{F}|$-partite.*

We define the *relative density* of $\mathcal{G}$ in Equation (36), which is the adaptation of the density of a graph to the conflict graph using Observation 3.1. This quantity is more meaningful, since it compares the number of edges of a conflict graph to the maximum number of edges a conflict graph could have.

$$d^*_{\mathcal{G}} = \frac{|\mathcal{E}|}{\frac{|\mathcal{V}|(|\mathcal{V}|-1)}{2} - \sum_{f \in \mathcal{F}} \frac{|\mathcal{M}_f|(|\mathcal{M}_f|-1)}{2}} \tag{36}$$

3.3 Conflict-free solution: Formulation and illustrative example

As mentioned in Section 1, given the current position, speed, acceleration and the planned trajectories of a set of aircraft, solving the CR problem consists in finding a conflict-free set of maneuvers that minimizes the total cost. Observation 3.2 links the cliques in $\mathcal{G}$ to the CR problem:

Observation 3.2 *Let $\mathcal{C}$ be a clique in graph $\mathcal{G}$. Then $\mathcal{C}$ represents a set of conflict-free maneuvers for a subset of $\mathcal{F}$ of cardinality $|\mathcal{C}|$.*

Observation 3.2 indicates that finding a set of conflict-free maneuvers for $\mathcal{F}$ is equivalent to finding a clique of $\mathcal{G}$ of cardinality $|\mathcal{F}|$. We derive the following proposition:

Proposition 3.3 *If a conflict-free solution exists, then $\omega(\mathcal{G}) = |\mathcal{F}|$. Otherwise, $\omega(\mathcal{G})$ is the maximum number of flights involved in a conflict-free situation.*

For the sake of clarity, an illustrative example with three aircraft and the corresponding solution are presented in Figure 5. If each aircraft follows its planned trajectory as indicated in Figure 5a, conflicts will happen between the blue aircraft and the two others. For this example, we assume that, in addition to the null maneuver, only two heading changes ($\pm 30°$) are allowed. We build the CR graph shown in Figure 5b. The graph is multipartite, each stable set representing the set of the possible maneuvers for one aircraft. Solving

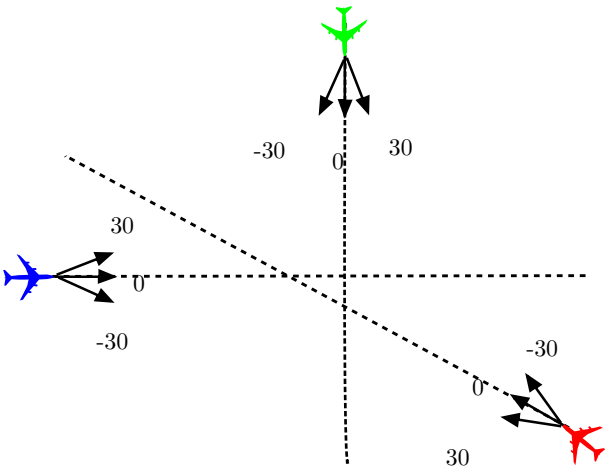

(a) Illustrative example with three aircraft

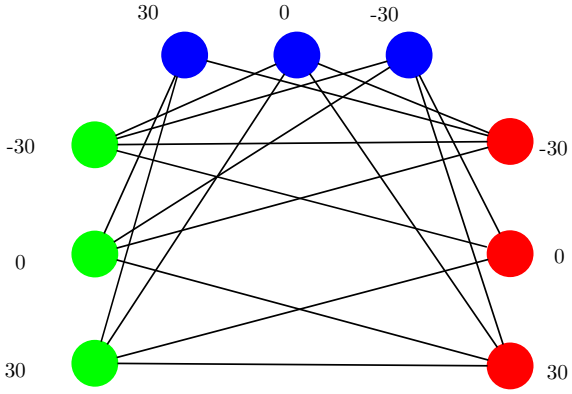

(b) Conflict graph $\mathcal{G}$ associated with the illustrative example

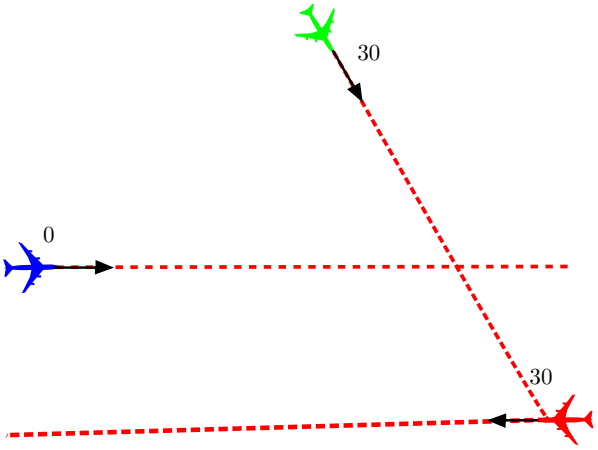

(c) Solution of the problem

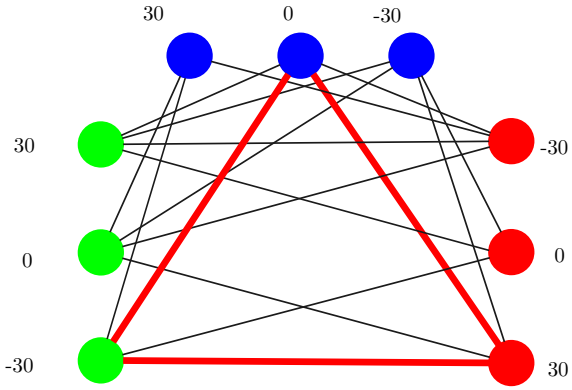

(d) Corresponding clique in the conflict graph $\mathcal{G}$

Figure 5: Illustrative example: instance and solution

the CR problem is then equivalent to searching for a minimum-weight clique of three vertices, i.e., a triangle. Figures 5c and 5d denote the corresponding solution and the triangle of minimum weight respectively.

We define the problem $\text{CR}_{\mathcal{M}}$ as the restriction of the CR problem to the set of maneuvers $\mathcal{M}$. Using both Observations 3.2 and 3.3, we can state anew the $\text{CR}_{\mathcal{M}}$ problem as follows: searching for a conflict-free solution of minimum cost is equivalent to solving the $\text{CR}_{\mathcal{M}}$ problem consisting of finding a clique of maximum cardinality and minimal cost in graph $\mathcal{G}$.

As stated in Subsection 2.2, the cost of a maneuver depends on the time during which it is executed. A first idea to model this would be to discretize this execution time and to create the vertices accordingly. Computing the cost of the vertices would be straightforward, using the method described in Subsection 2.2. The drawback of this method is the explosion of the number of vertices, which will drastically increase the runtime of any solution algorithm. To address this issue, we decided to maintain the graph small by considering one vertex per maneuver. By making this choice, the cost of the vertices cannot be determined *a priori* anymore, since it depends on the maneuvers executed by the other aircraft. In other words, the cost of each vertex depends on the vertices in the clique. This problem is a new variant of the maximum clique of minimum weight problem, where even though the weights considered are on the vertices, these weights depend on the vertices in the clique.

3.4 Computing the costs

For a more synthetic presentation, and without loss of generality, no distinction is made between a vertex and the corresponding maneuver in this subsection. As explained in the previous subsection, the cost of a maneuver depends on its execution, which itself varies with the maneuvers performed by the other aircraft. As a consequence, we need to define the cost of the edges before the cost of the vertices.

3.4.1 Cost of the edges

For a more synthetic presentation, an edge $e = (i, j)$ will be considered as a pair of maneuvers. We compute the cost of an edge $e = (i, j)$ as a pair constituted of the cost of maneuvers i and j, denoted $C_i^{(i,j)}$ and $C_j^{(i,j)}$. These costs correspond to an execution time t_i^j which is the minimum time during which i and j have to be executed before a safe return can be performed by at least one of the aircraft.

3.4.2 Cost of the vertices

Let us consider a maneuver i. To determine the cost of i, denoted c_i, we need to compute the time t_i during which it is actually applied. If i is not in the optimal solution, then $t_i = 0$. Otherwise, t_i is given by

$$t_i = \max_{j \in \mathcal{V} \cap \mathcal{C}} t_i^j \tag{37}$$

Equation (37) states that maneuver i has to be applied long enough in order to be conflict-free with every other chosen maneuvers. Indeed, if aircraft i and j are conflict-free when they execute their maneuvers during a duration t, then they will remain conflict-free if they perform their maneuvers during $T > t$.

We can determine c_i:

$$c_i = \begin{cases} \max\limits_{j \in \mathcal{V} \cap \mathcal{C}} C_i^{(i,j)} & \text{if } i \in \mathcal{C} \\ 0 & \text{otherwise} \end{cases}$$

4 Methodology

4.1 MILP formulation

4.1.1 Motivations

Finding a maximum clique in an arbitrary graph is a well-known optimization problem that is among the $\mathcal{NP}$-hard problems enumerated by Karp [34]. Due to its high complexity, the problem has been thoroughly studied and several methods, both exact and heuristic, have been developed. For a comprehensive coverage of the theoretical results, complexity study and existing methods overview, one can refer to Bomze et al. [35] and Hao et al. [36].

In the cited methods, the weight of the vertices are known beforehand and are data of the problem. However, in our model the costs of the vertices are not determined *a priori*, since they depend on which vertices are in the clique. As a consequence, the dedicated algorithms of existing graph theory libraries cannot be used in this study. To address this issue, we formulate our problem as a MILP that can be solved with any generic MILP solver.

4.1.2 Formulation

The decision variables of the model all relate to the vertices of the graph. They correspond to the choice of the vertices in the clique and the cost of each vertex:

- $x_i = \begin{cases} 1 & \text{if vertex } i \text{ is part of the maximum clique} \\ 0 & \text{otherwise} \end{cases}$

- $c_i \in \mathbb{R}_+$ is the cost of vertex i.

The clique search can then be modeled as the following MILP, denoted MIP:

$$\text{minimize} \sum_{i \in \mathcal{V}} c_i \tag{38}$$

$$\text{subject to } x_i + x_j \leq 1, \forall (i,j) \notin \mathcal{E} \tag{39}$$

$$\sum_{i \in \mathcal{V}} x_i = N \tag{40}$$

$$c_i \geq C_i^{(i,j)}(x_i + x_j - 1), \forall (i,j) \in \mathcal{E} \tag{41}$$

$$x_i \in \{0;1\}, \forall i \in \mathcal{V} \tag{42}$$

$$c_i \in \mathbb{R}_+, \forall i \in \mathcal{V} \tag{43}$$

The objective function (38) minimizes the cost of the maneuvers. Constraints (39) are clique constraints stating that two nonadjacent vertices must not be part of the clique. In terms of conflict resolution, it means that two maneuvers in conflict must not be part of the solution. Constraint (40) exploits Proposition 3.3 defining the cardinality of the maximum clique. Constraints (41) are used to compute the cost of the vertices: if a vertex is in the maximum clique, then its cost must be greater than the cost on every edge connecting it to other vertices in the clique. Otherwise, no particular constraint is imposed on the vertex cost. Constraints (42)–(43) are binarity and positivity constraints, respectively.

4.1.3 Strengthening the linear relaxation

Strengthening the linear relaxation of a MILP can yield improvements for the resolution. Indeed, it allows the explored branch-and-bound nodes to have a better lower bound. We tightened the linear relaxation by including the following constraints in our model:

$$\sum_{j \in \mathcal{V}_f} x_j = 1, \forall f \in \mathcal{F} \tag{44}$$

Constraints (44) simply illustrate that each aircraft must be assigned a maneuver. These constraints were not included in the original formulation, since the constraints (39), (40) and (42) make them redundant. Indeed, each set of nodes $\mathcal{M}_f$ is a stable, meaning that only one maneuver can be assigned to each aircraft in a clique. Since (40) requires that the number of vertices in the clique is equal to the number of aircraft, (44) is always satisfied in a solution of (39)–(43). However these constraints improve the linear relaxation of the MILP, because they prevent it from considering a solution where the fractional maneuvers are all assigned to the same aircraft.

4.2 Decomposition methods

The motivations for the design of decomposition methods are two-fold. First, as the MWMCC problem is known to be $\mathcal{NP}$-hard, an increase in solution time with the size of the instances can be expected. Moreover, the size of the sets of maneuvers can also impact the required computational effort. Second, in practice the instances have important inherent geometric characteristics. Indeed, aircraft evolving on different flight levels are weakly interdependent, meaning that they will almost never interfere with each other. However, these geometric considerations do not appear explicitly in our model.

To address these observations, we design two decomposition methods. The analyze of the answers to the observations provided by the methods will be discussed in Section 5.

4.2.1 SMILO procedure

In this subsection, we present a SMILO procedure for the CR problem. This procedure iteratively solves several MILPs on graphs having the same number of vertices, but where the discretization values are updated

in a fashion similar to a trust region method. The motivations behind the design of this procedure is to obtain a trade-off between the solution time and cost, and to study the impact of the chosen discretization. Algorithm 1 describes the mechanics of the SMILO procedure.

Algorithm 1 SMILO procedure for the CR problem

procedure SMILO($\mathcal{F}, v^1_{\min}, ..., v^N_{\min}, v^1_{\max}, ..., v^N_{\max}, ..., \chi^1_{\min}, \chi^N_{\min}, \chi^1_{\max}, ..., \chi^N_{\max}, \delta^1_v, ..., \delta^N_v, \delta^1_\chi, ..., \delta^N_\chi$)
  for $f \in \mathcal{F}$ **do**
    $n^f_v \leftarrow \frac{v^f_{\max} - v^f_{\min}}{\delta^f_v}$
    $n^f_\chi \leftarrow \frac{\chi^f_{\max} - \chi^f_{\min}}{\delta^f_\chi}$
  $z_c \leftarrow +\infty$
  while $|z - z_c| > 0.01$ **do**
    $z \leftarrow z_c$
    $z \leftarrow SOLVE\_MIP(\mathcal{F}, v^1_{\min}, ..., v^N_{\min}, v^1_{\max}, ..., v^N_{\max}, ..., \chi^1_{\min}, ..., \chi^N_{\min}, \chi^1_{\max}, ..., \chi^N_{\max}, \delta^1_v, ..., \delta^N_v, \delta^1_\chi, ..., \delta^N_\chi)$
    if $z < +\infty$ **then**
      for $f \in \mathcal{F}$ **do**
        Let m be the maneuver of aircraft f in the last solution found
        if m is the null maneuver **then**
          Erase all the heading and speed nodes of aircraft f
          $\chi^f_{\max} \leftarrow \lfloor \frac{n^f_\chi}{2} \rfloor$
          $\chi^f_{\min} \leftarrow -\chi^f_{\max}$
          $\delta^f_\chi \leftarrow 1$
          Build heading nodes with the values of $\chi^f_{\max}, \chi^f_{\min}$ and δ^f_χ
          $v^f_{\max} \leftarrow \lfloor \frac{n^f_v}{2} \rfloor$
          $v^f_{\min} \leftarrow -v^f_{\max}$
          $\delta^f_v \leftarrow 1$
          Build speed nodes with the values of $v^f_{\max}, v^f_{\min}$ and δ^f_v
        else
          if m is a heading maneuver **then**
            Erase all speed nodes of aircraft f
            $\chi^f_{\max} \leftarrow \max\{m, 0\}$
            $\chi^f_{\min} \leftarrow \min\{m, 0\}$
            $\delta^f_\chi \leftarrow \lfloor \frac{|m|}{n^f_\chi} \rfloor$
            Build heading nodes with the values of $\chi^f_{\max}, \chi^f_{\min}$ and δ^f_χ
          else
            Erase all heading nodes of aircraft f
            $v^f_{\max} \leftarrow \max\{m, 0\}$
            $v^f_{\min} \leftarrow \min\{m, 0\}$
            $\delta^f_v \leftarrow \lfloor \frac{|m|}{n^f_v} \rfloor$
            Build speed nodes with the values of $v^f_{\max}, v^f_{\min}$ and δ^f_v
    else
      for $f \in \mathcal{F}$ **do**
        $v^f_{\max} \leftarrow 2v^f_{\max}$, $\chi^f_{\max} \leftarrow 2\chi^f_{\max}$, $v^f_{\min} \leftarrow 2v^f_{\min}$, $\chi^f_{\min} \leftarrow 2\chi^f_{\min}$, $\delta^f_v \leftarrow 2\delta^f_v$, $\delta^f_\chi \leftarrow 2\delta^f_\chi$
      $z_c \leftarrow SOLVE\_MIP(\mathcal{F}, v^1_{\min}, ..., v^N_{\min}, v^1_{\max}, ..., v^N_{\max}, ..., \chi^1_{\min}, ..., \chi^N_{\min}, \chi^1_{\max}, ..., \chi^N_{\max}, \delta^1_v, ..., \delta^N_v, \delta^1_\chi, ..., \delta^N_\chi)$

The parameters describe a conflict graph with the following features:

- $\mathcal{F}$: the set of aircraft;
- $v^f_{\min}, v^f_{\max}$: minimum and maximum speed deviation allowed for aircraft f;
- $\chi^f_{\min}$, $\chi^f_{\max}$: minimum and maximum heading deviation allowed for aircraft f;
- $\delta^f_v, \delta^f_\chi$: speed and heading discretization of the maneuvers of aircraft f;
- n^f_s, n^f_χ: number of speed and heading nodes aircraft f. The values are computed using the values of $v^f_{\min}, v^f_{\max}, \chi^f_{\min}, \chi^f_{\max}, \delta^f_v$ and δ^f_χ.

The procedure starts by storing the number of vertices representing speed and heading maneuvers for each aircraft. It sequentially solves MIP until no improvement is achieved while updating the set of nodes $\mathcal{M}$ between two consecutive resolutions. The update of the vertices $\mathcal{M}$ depends on whether or not the current instance of the graph is feasible. If it is feasible, the update varies with the maneuver assigned to f in the current solution:

- if f perfoms no maneuver, $\mathcal{M}_f$ is erased, except for the NIL node. New sets of speed and heading maneuvers are added to $\mathcal{F}$ in order to obtain intervals centered around 0;
- if f performs a heading change of magnitude m, all the speed nodes are deleted from $\mathcal{M}_f$ and the heading interval is replaced with another interval having 0 and m as extremums. The discretization step is chosen in order to keep n_χ^f heading nodes;
- if f performs a speed change of magnitude m, all the heading nodes are deleted from $\mathcal{M}_f$ and the speed interval is replaced with another interval having 0 and m as extremums, depending on the sign of m. The discretization step is chosen in order to keep n_v^f speed nodes.

In the situation where the current instance is not feasible, all the parameters describing the maneuvers $\mathcal{F}$ are doubled, in order to allow for larger maneuvers while maintaining a constant number of vertices in the graph.

4.2.2 Second decomposition method

The decomposition method is inspired from the POPMUSIC algorithm developed by Taillard and Voß [37]. This meta-heuristic is applied to various combinatorial optimization problems that can be partially optimized. It was designed to address the limitations of local search methods applied to problems of large size. It provides a method generating neighborhoods that are a better fit for these problems. These neighborhoods need not being enumerated, since they can be implicitly explored with an optimization procedure. Algorithm 2 details the mechanics of the method.

Algorithm 2 Large Neighborhood Search (LNS) Algorithm

```
1:  procedure LNS(r)
2:      Input: Solution S composed of parts s_1, ..., s_p
3:      O ← ∅
4:      while O ≠ {s_1, ..., s_p} do
5:          Select s_i ∉ O
6:          Create a subproblem R_i composed of the r parts {s_{i_1}, ..., s_{i_r}} most related to s_i
7:          Optimize R_i
8:          if R_i has been improved then
9:              Update S
10:             O ← ∅
11:         else
12:             O ← O ∪ {s_i}
```

To apply Algorithm 2, the user needs to define four key elements:

1. the definition of the parts of a solution;
2. the selection procedure in O;
3. the definition of relatedness between solution parts;
4. the sub-problem optimizer.

The algorithm works on a solution divided into p parts. While some parts still need to be selected, the algorithm selects a part p_0 to be optimized. To this end, a subproblem is created with the r parts of the

solution that are the most related to p_0 . If the subproblem yields an improvement of p_0 , then all parts can be selected again. Otherwise, p_0 cannot be chosen again.

In a nutshell, the algorithm iteratively tries to improve the current solution by performing several neighborhood searches to improve every part of the solution. The neighborhood of a part of the solution is defined according to a relatedness criterion defined by the user.

We apply Algorithm 2 to large instances with aircraft randomly generated on different flight levels. We design the above-mentioned points as follows:

1. A solution part per flight level;
2. the selection procedure in O is the lowest flight level in O;
3. the relatedness between solution parts is defined as the vertical distance between their corresponding flight level;
4. the sub-problem optimizer is Algorithm 1.

Algorithm 3 gives the details of the overall procedure. The set of aircraft is sorted by flight level. A first loop is performed, where for each flight level, Algorithm 1 is used to optimize the problem for the corresponding aircraft, but allowing only horizontal maneuvers. In the second part of the algorithm (corresponding to the *while* loop), for each flight level, Algorithm 1 is used to optimize the problem for the corresponding aircraft. The difference is that they can change of flight level, but the constraints take into account the maneuvers of the set of aircraft on the adjacent levels. In other words, we authorize all types of maneuvers on the flight level, but we fix the maneuvers of the aircraft on adjacent levels to those that appear in the last solution found. Algorithm 3 stops when no improvement is achieved.

Algorithm 3 Spatial decomposition method

procedure SPATIAL_ DECOMPOSITION($\mathcal{F}$)
  Input: $\mathcal{F}$: set of aircraft randomly generated on p flight levels
  for $i = 1, \ldots, p$ **do**
    Solve conflicts for flight level i without altitude maneuvers
    $s_i \leftarrow$ result of the resolution for flight level i
Call LNS(2)
  Input: Solution S composed of parts $s_1, \ldots, s_p$
  R_1: solve conflicts for Flight Level (FL) 1 allowing altitude maneuvers, given the maneuvers of s_2
  R_p: solve conflicts for FL p allowing altitude maneuvers, given the maneuvers of s_{p-1}
  for $i = 2, \ldots, p-1$ **do**
    R_i: solve conflicts for FL i allowing altitude maneuvers, given the maneuvers of s_{i-1} and s_{i+1}

For this study, we apply Algorithm 3 to instances with aircraft randomly spread on several flight levels. However, Algorithm 3 could be applied to other type of instances. The only thing to adapt is the relatedness between subsets of aircraft, which would divide the set of aircraft into different clusters.

5 Results

In this section, the proposed model is validated with a benchmark of structured instances known in the literature as complex to solve, both two-dimensional and three-dimensional. The data that was used to compute the maneuvers and their costs were all extracted from the BADA table that refers to the Airbus A-320. All tests were performed on a computer equipped with the following hardware: Intel Core i7-3770 processor, 3.4 GHz, 8-GB RAM. The algorithms were implemented in C++ and relies on CPLEX 12.5.1.0 [38] with default options to solve every instance.

The tables presented in this section gather information about the problems dimensions and computational results. The headings are given as follows:

- *Case*: case configuration;
- $|\mathcal{F}|$: number of aircraft;
- $|\mathcal{V}|$: number of vertices;
- $|\mathcal{E}|$: number of edges;
- d^*: relative graph density;
- n: number of variables;
- m: number of constraints;
- z_{ip}: optimal value of the problem (in kilograms of fuel);
- n_{nodes}: number of branch-and-bound nodes;
- t_{lp}: time (in seconds) to solve the continuous relaxation of the MILP;
- t_{ip}: time (in seconds) to obtain the z_{ip} value.

5.1 Benchmark description

5.1.1 Structured instances

This benchmark gathers three types of instances. The first ones are roundabout instances $\mathcal{R}_n$, where n aircraft are distributed on the circumference of a 100NM radius and fly towards the center at the same speed and altitude. The second set gathers crossing flow instances $\mathcal{F}_{n,\theta,d}$, where two trails of n aircraft separated by d nautical miles intersect each other with an angle θ. The last type of instances are grids $\mathcal{G}_{n,d}$ constituted of two flow instances $\mathcal{F}_{n,\frac{\pi}{2},d}$, one instance being translated 15NM North-East from the other. One example of each type of instance is given on Figure 6.

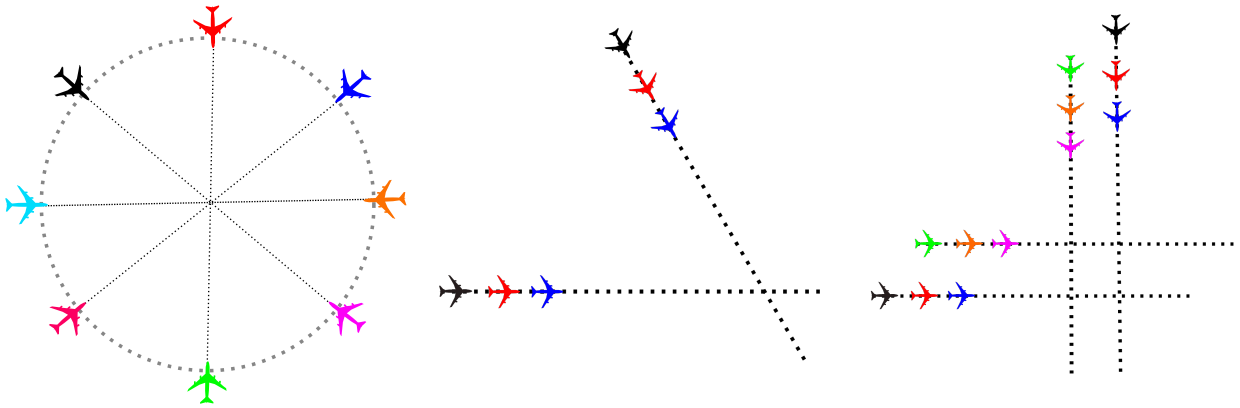

(a) Roundabout (b) Crossing Flow (c) Grid

Figure 6: Examples

5.1.2 Single-level random benchmark

This benchmark consists of random instances, where aircraft are uniformely distributed within a square sector with side length 50NM. To avoid generating infeasible instances, we perform a preprocessing before solving the problem: for each pair of aircraft that will loose separation within the first 30 seconds of observation, we randomly delete one of the two aircraft. For a desired number of aircraft, we generate 15% more aircraft to anticipate the effect of the preprocessing. If more aircraft than desired remain after the preprocessing, extra aircraft are randomly removed until the desired number is reached.

5.1.3 Multi-level benchmark

We design this benchmark to study instances closer to the operational context. We generate a larger number of aircraft than for the single-level benchmark (from 50 to 200 aircraft with increments of 25 aircraft). The

generation of aircraft is performed following the same procedure as for the single-level case. The aircraft are later randomly assigned to the different flight levels, following a uniform distribution. We denote $\mathcal{M}_{n,m}$ the instance where n aircraft are assigned to m different flight levels.

5.2 Computational results

5.2.1 Structured instances

Solutions for the instances described in Figure 6 are displayed on Figure 7. Figure 7a depicts the optimal solution for the instance $\mathcal{R}_8$ where all aircraft perform a right turn of 5° and avoid each other in a roundabout fashion before returning to their initial trajectory. Instance $\mathcal{F}_{3,\frac{\pi}{4},10}$ is solved in a symmetric fashion: each trail of aircraft perform the same set of heading changes. The first aircraft of each trail turns right by 5°, while the second and third aircraft turn left by 5° and 10° respectively. Instance $\mathcal{G}_{3,10}$ is also solved symmetrically, where the horizontal trails follow the same set of maneuvers, as well as the vertical trails.

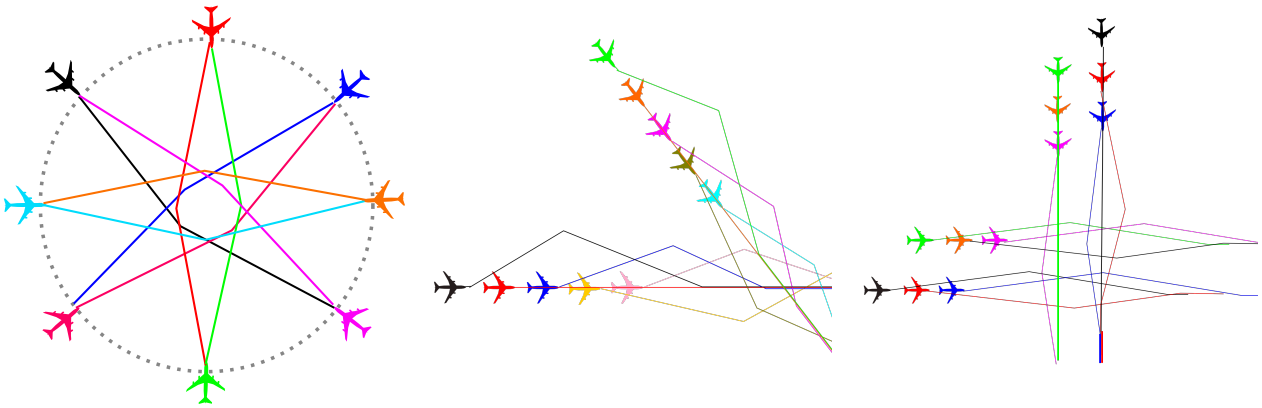

(a) Roundabout (b) Crossing Flow (c) Grid

Figure 7: Solutions of the examples

The first set of simulations considers only horizontal maneuvers, with relative speed changes of $\pm 2\%$, $\pm 4\%$ and $\pm 6\%$ and heading changes of $\pm 5°, \pm 10°, \pm 15°$. Table 1 gathers the main information about the dimensions of the instances, along with the computational results of the original model. Results of the SMILO procedure on these instances are gathered in Subsection 5.3. Algorithm 3 was not applied to this benchmark because the symmetry inherent to the instances make the design of a relatedness procedure not necessarily relevant.

The original model yields the optimal solution in real-time. Indeed, problems known to be complex with up to 20 aircraft are solved to optimality in less than 15 seconds. This result is very satisfying since the density of the graph is high.

In the second simulation set, we introduce altitude maneuvers: aircraft are allowed to move to an adjacent flight level. Table 2 reports the main results. Solution times tend to slightly increase. This is explained by the introduction of a new set of high degree vertices. Indeed, every change of flight level is conflict-free with all the horizontal maneuvers. Nevertheless, the solution can still be computed in a short time. These results are promising since the tested instances involve a denser traffic than real-life situations.

5.2.2 Single-level random benchmark

Figure 8a displays a randomly chosen instance $\mathcal{U}_{15}$ along with the corresponding solution on Figure 8b. Initial speed vectors are represented by dotted vectors, whereas requested maneuvers are given by solid vectors. The two aircraft circled in red changed their flight level.

Table 1: Dimensions of the instances and computational results for the virtual benchmark using only horizontal maneuvers

		Graph $\mathcal{G}$				MILP		Resolution			
Instance type	Case	$\lvert\mathcal{F}\rvert$	$\lvert\mathcal{V}\rvert$	$\lvert\mathcal{E}\rvert$	d	m	n	z_{ip}	$nodes$	t_{lp}	t_{ip}
Roundabout	$\mathcal{R}_4$	4	52	612	0.6	104	1333	2.66	27	0.02	0.07
	$\mathcal{R}_8$	8	104	2744	0.58	208	5705	5.34	75	0.02	0.51
	$\mathcal{R}_{12}$	12	156	6300	0.56	312	12925	19.99	84	0.02	2.95
	$\mathcal{R}_{16}$	16	208	11396	0.56	416	23225	42.73	39	0.02	6.99
	$\mathcal{R}_{20}$	20	260	17756	0.55	520	36053	86.59	71	0.02	11.63
Flows	$\mathcal{F}_{1,60,10}$	2	26	102	0.6	52	259	1.32	0	0.02	0.05
	$\mathcal{F}_{2,60,10}$	4	52	736	0.73	104	1581	2.66	0	0.02	0.06
	$\mathcal{F}_{3,60,10}$	6	78	1980	0.78	156	4123	4	0	0.02	0.18
	$\mathcal{F}_{4,60,10}$	8	104	3846	0.81	208	7909	5.34	57	0.02	0.57
	$\mathcal{F}_{5,60,10}$	10	130	6349	0.83	260	12969	6.68	0	0.02	0.9
	$\mathcal{F}_{6,60,10}$	12	156	9483	0.85	312	19291	9.96	70	0.02	1.96
	$\mathcal{F}_{7,60,10}$	14	182	13252	0.86	364	26883	13.3	0	0.02	1.44
	$\mathcal{F}_{8,60,10}$	16	208	17659	0.87	416	35751	18.66	0	0.02	1.7
	$\mathcal{F}_{9,60,10}$	18	234	19057	0.88	468	42579	30.18	10	0.02	1.79
	$\mathcal{F}_{10,60,10}$	20	260	22563	0.87	520	47264	41.61	0	0.02	1.85
Grids	$\mathcal{G}_{2,1,10}$	4	52	787	0.78	104	1683	1.32	35	0.02	0.18
	$\mathcal{G}_{2,2,10}$	8	104	3780	0.8	208	7777	3.33	0	0.02	0.28
	$\mathcal{G}_{2,3,10}$	12	156	9072	0.81	312	18469	6.01	29	0.02	1.98
	$\mathcal{G}_{2,4,10}$	16	208	16854	0.83	416	34141	11.23	55	0.02	5.87
	$\mathcal{G}_{2,5,10}$	20	260	27207	0.85	520	54955	16.06	138	0.02	13.59

Table 2: Dimensions of the instances and computational results on the virtual benchmark including flight level changes

		Graph $\mathcal{G}$				MILP		Resolution			
Instance type	Case	$\lvert\mathcal{F}\rvert$	$\lvert\mathcal{V}\rvert$	$\lvert\mathcal{E}\rvert$	d	m	n	z_{ip}	$nodes$	t_{lp}	t_{ip}
Roundabout	$\mathcal{R}_4$	4	60	936	0.69	120	1997	2.66	0	0.02	0.08
	$\mathcal{R}_8$	8	120	4256	0.68	240	8761	5.34	67	0.02	0.7
	$\mathcal{R}_{12}$	12	180	9864	0.66	360	20101	19.99	108	0.02	4.27
	$\mathcal{R}_{16}$	16	240	17876	0.66	480	36249	42.73	96	0.02	16.63
	$\mathcal{R}_{20}$	20	300	28016	0.66	600	56653	86.59	277	0.02	37.1
Flows	$\mathcal{F}_{1,60,10}$	2	30	156	0.69	60	375	1.32	0	0.02	0.02
	$\mathcal{F}_{2,60,10}$	4	60	1068	0.79	120	2261	2.66	54	0.02	0.22
	$\mathcal{F}_{3,60,10}$	6	90	2814	0.83	180	5815	4	0	0.02	0.23
	$\mathcal{F}_{4,60,10}$	8	120	5406	0.86	240	11061	5.34	75	0.02	0.98
	$\mathcal{F}_{5,60,10}$	10	150	8859	0.87	300	18029	6.68	0	0.02	1.19
	$\mathcal{F}_{6,60,10}$	12	180	13167	0.89	360	26707	9.96	74	0.02	2.4
	$\mathcal{F}_{7,60,10}$	14	210	18334	0.9	420	37103	13.3	123	0.02	3.6
	$\mathcal{F}_{8,60,10}$	16	240	24363	0.9	480	49223	18.66	103	0.02	7.2
	$\mathcal{F}_{9,60,10}$	18	270	31261	0.91	540	63081	30.18	79	0.02	9.13
	$\mathcal{F}_{10,60,10}$	20	300	39036	0.91	600	78693	41.61	92	0.02	11.51
Grids	$\mathcal{G}_{2,1,10}$	4	60	1115	0.83	120	2355	1.32	53	0.02	0.1
	$\mathcal{G}_{2,2,10}$	8	120	5332	0.85	240	10913	3.33	0	0.02	0.42
	$\mathcal{G}_{2,3,10}$	12	180	12744	0.86	360	25861	6.01	0	0.02	2.01
	$\mathcal{G}_{2,4,10}$	16	240	23542	0.87	480	47581	11.23	185	0.02	10.05
	$\mathcal{G}_{2,5,10}$	20	300	37807	0.87	600	76235	16.06	180	0.02	19.91

The computational results are reported in Table 3. Figures displayed are averages over 100 simulations.

Table 4 displays the computational results for the single-level random benchmark with the addition flight level changes: aircraft can climb to the next level or descend to the one underneath.

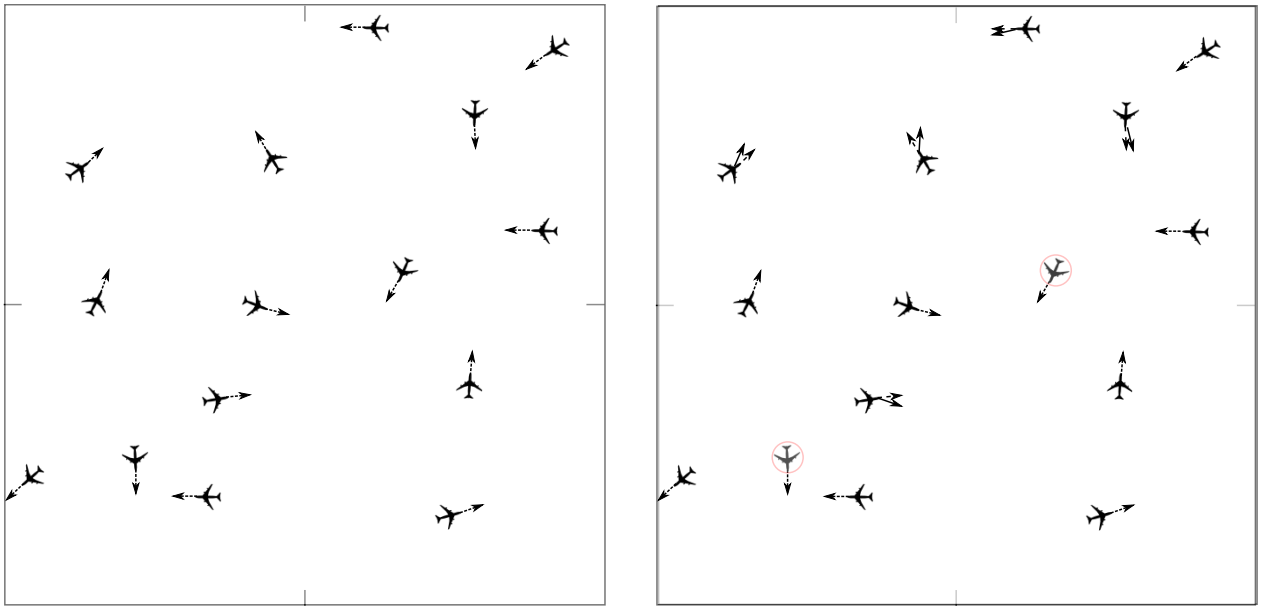

(a) Random instance (b) Solution

Figure 8: Random instance $\mathcal{U}_{15}$ and its solution

Table 3: Dimensions of the instances and computational results on the single-level random benchmark including horizontal maneuvers

		Graph $\mathcal{G}$				MILP		Resolution			
Instance type	Case	$\lvert\mathcal{F}\rvert$	$\lvert\mathcal{V}\rvert$	$\lvert\mathcal{E}\rvert$	d	m	n	z_{ip}	$nodes$	t_{lp}	t_{ip}
Random	$\mathcal{U}_5$	5	55	726	1	110	1567	0.05	0	0.02	0
	$\mathcal{U}_{10}$	10	110	4830	0.99	220	9890	0.23	0	0.02	0
	$\mathcal{U}_{15}$	15	165	9865	0.99	330	20075	0.86	0	0.02	7.56
	$\mathcal{U}_{20}$	20	220	14365	0.99	440	29190	1.54	8	0.02	11.1
	$\mathcal{U}_{25}$	25	275	19182	0.98	550	38939	2.15	19	0.02	12.1
	$\mathcal{U}_{30}$	30	330	28750	0.99	660	58190	2.21	45	0.02	14.32
	$\mathcal{U}_{35}$	35	385	31406	0.99	770	63617	2.41	75	0.02	16.25
	$\mathcal{U}_{40}$	40	440	52766	0.99	880	106452	3.21	119	0.02	19.63
	$\mathcal{U}_{45}$	45	495	62051	0.99	990	125137	3.26	179	0.02	20.02
	$\mathcal{U}_{50}$	50	550	57215	1	1100	115580	3.87	225	0.02	20.06
	$\mathcal{U}_{55}$	55	605	69090	0.99	1210	139445	4.83	346	0.02	22.21
	$\mathcal{U}_{60}$	60	660	75338	0.98	1320	152056	6.32	561	0.02	29.35

The computational time remains short, but for some generated instances it tends to increase. To investigate this issue, we ran other simulations while changing the number of possible maneuvers. Results highlighted a high sensitivity of the computational time of the model regarding the number of vertices for a given instance. This observation is at the core of the design of the SMILO procedure presented in Subsection 4.2.

5.3 Detailed results for the SMILO procedure on the benchmark without altitude changes

This simulation set was designed to address two points of investigation. The first one is to identify the impact of the number of maneuvers on the objective function and the computational time. The second one was to evaluate the performances of the SMILO procedure, and to classify it in terms of trade-off between the optimal value and the computational time.

Table 4: Dimensions of the instances and computational results on the single-level random benchmark including horizontal maneuvers and flight level changes

		Graph $\mathcal{G}$				MILP		Resolution			
Instance type	Case	$\lvert\mathcal{F}\rvert$	$\lvert\mathcal{V}\rvert$	$\lvert\mathcal{E}\rvert$	d	m	n	z_{ip}	$nodes$	t_{lp}	t_{ip}
Random	$\mathcal{U}_5$	5	75	1209	1	150	2573	0.01	0	0.02	0.01
	$\mathcal{U}_{10}$	10	150	4839	1	300	9988	0.01	0	0.02	7.07
	$\mathcal{U}_{15}$	15	225	8939	0.98	450	18343	0.32	0	0.02	15.25
	$\mathcal{U}_{20}$	20	300	16732	0.99	600	34084	0.97	0	0.02	18.55
	$\mathcal{U}_{25}$	25	375	22345	0.98	750	45465	1.29	38	0.02	20.55
	$\mathcal{U}_{30}$	30	450	32248	0.99	900	65426	1.37	31	0.02	21.46
	$\mathcal{U}_{35}$	35	525	42027	0.99	1050	85139	1.76	0	0.02	25.22
	$\mathcal{U}_{40}$	40	600	50386	0.99	1200	102012	2.04	0	0.02	29.15
	$\mathcal{U}_{45}$	45	675	60764	0.99	1350	122923	3.18	41	0.02	34.02
	$\mathcal{U}_{50}$	50	750	69035	0.99	1500	139620	3.12	0	0.02	37.47
	$\mathcal{U}_{55}$	55	825	84344	0.99	1650	170393	4.55	89	0.02	40.16
	$\mathcal{U}_{60}$	60	900	75126	0.99	1800	152112	6.24	26	0.02	55.25

These simulations were ran with four different parameter sets:

- a large discretization, with relative speed changes of $\pm 6\%$ and heading changes of $\pm 15°$, yielding an objective function value z^l_{ip} within time t^l_{ip};
- a medium discretization, with relative speed changes of $\pm 2\%$, $\pm 4\%$ and $\pm 6\%$ and heading changes of $\pm 5°, \pm 10°, \pm 15°$m, yielding an objective function value z^m_{ip} within time t^m_{ip};
- a narrow discretization, with 12 relative speed changes between -6% and 6% with a step of 1% and heading changes between $-15°$ and $15°$ with a step of $1°$. These parameters yield an objective function value z^n_{ip} within time t^n_{ip};
- the SMILO procedure applied with four speed changes and four heading changes, yielding an objective function value z_{SMILO} within time t_{SMILO}.

Table 5 gathers the main results of these simulations. Results exhibit that the choice of the discretization size is critical regarding the computational time. Indeed, going from a medium discretization to a narrow discretization divides on average the cost of the solution by 2, but the solution time is on average 18 times longer. Results for the SMILO procedure evidence that it represents a good trade-off between finding an efficient solution while not taking too much time. Indeed, solutions found by the SMILO procedure are on average 41% more expensive than the medium discretization ones, but it takes 50% less time to find them. This result is especially useful for the random instances, where the original optimization model seemed less efficient.

Figure 9 depicts a visual summary of Table 5. Figure 9a highlights the influence of the discretization on the quality of the best solution found, and compares the solution found by the SMILO procedure to those obtained with the different discretizations. Results place the SMILO solution as an intermediate between the large and medium discretization solutions. Figure 9b compares the solution time of the SMILO procedure with that yielded by the small and medium discretizations. The solution times with the small discretization were not displayed on the chart, since those values are not of the same scale. Results show that the SMILO procedure needs less time than the model with the medium discretization in order to find the optimal value regarding the available set of maneuvers.

5.3.1 Evaluating the second decomposition method on the multi-level random benchmark

Table 6 gathers the computational results of the second decomposition method on the multi-level random benchmark. In order to study the performances of the method, we compare it with the classical model. z_{ip} (respectively t_{ip}) correspond to the optimal value (respectively CPU time) of the second decomposition method using the first one as a subroutine. z^f_{best} (respectively t^f_{best}) denote the best value (respectively the

Table 5: Dimensions of the instances and computational results

Instance type	Case	Large discretization		Medium discretization		Small disctretization		Iterative procedure		
		z^l_{ip}	t^l_{ip}	z^m_{ip}	t^m_{ip}	z^n_{ip}	t^n_{ip}	z_{SMILO}	t_{SMILO}	CPLEX Calls
Roundabout	$\mathcal{R}_4$	7.93	0.04	2.66	0.07	0.96	1.45	1.06	0.06	4
	$\mathcal{R}_8$	18.64	0.25	5.34	0.51	5.34	69.2	6.42	0.26	4
	$\mathcal{R}_{12}$	32.03	0.72	19.99	2.95	15.71	362.06	18.03	0.75	3
	$\mathcal{R}_{16}$	42.73	2.37	42.73	6.99	38.67	2414.48	42.73	2.41	3
	$\mathcal{R}_{20}$	132.65	10.59	86.59	11.63	76.56	1162.29	86.59	10.39	4
Flows	$\mathcal{F}_{1,60,10}$	2.58	0.01	1.32	0.05	0.47	0.45	0.67	0.02	3
	$\mathcal{F}_{2,60,10}$	5.26	0.03	2.66	0.06	1.14	1.27	4.09	0.04	3
	$\mathcal{F}_{3,60,10}$	7.93	0.08	4	0.18	2	9.33	2.32	1.11	4
	$\mathcal{F}_{4,60,10}$	10.61	0.17	5.34	0.57	3.09	48.51	7.53	1.19	4
	$\mathcal{F}_{5,60,10}$	13.29	0.43	6.68	0.9	4.43	157.62	9.22	1.54	4
	$\mathcal{F}_{6,60,10}$	18.64	0.82	9.96	1.96	6.35	681.09	12.39	1.82	3
	$\mathcal{F}_{7,60,10}$	24	0.9	13.3	1.44	9.35	2431.05	14.45	1.95	4
	$\mathcal{F}_{8,60,10}$	29.35	0.77	18.66	1.7	14.67	3600.25	18.01	1.82	4
Grids	$\mathcal{G}_{2,1,10}$	5.26	0.04	1.32	0.18	0.69	1.95	1.32	0.05	3
	$\mathcal{G}_{2,2,10}$	10.61	0.18	3.33	0.28	1.39	14.93	1.44	0.26	4
	$\mathcal{G}_{2,3,10}$	15.97	0.64	6.01	1.98	2.41	62.33	3.41	6.96	6
	$\mathcal{G}_{2,4,10}$	25.17	2.77	11.23	5.87	3.61	317.8	11.14	13.21	3
	$\mathcal{G}_{2,5,10}$	37.3	4.5	16.06	13.59	5.48	1845.36	17.51	17.72	5
Random	$\mathcal{U}_{15}$	1.37	8.12	0.54	9.1	0.34	118.45	0.56	11.34	3
	$\mathcal{U}_{30}$	3.34	10.03	2.21	12.32	1.02	500.12	2.31	14.26	4
	$\mathcal{U}_{45}$	5.12	14.32	3.26	19.02	2.97	1002.87	3.27	22.6	6
	$\mathcal{U}_{60}$	8.45	17.01	6.32	23.35	5.98	1237.12	6.32	29.18	3

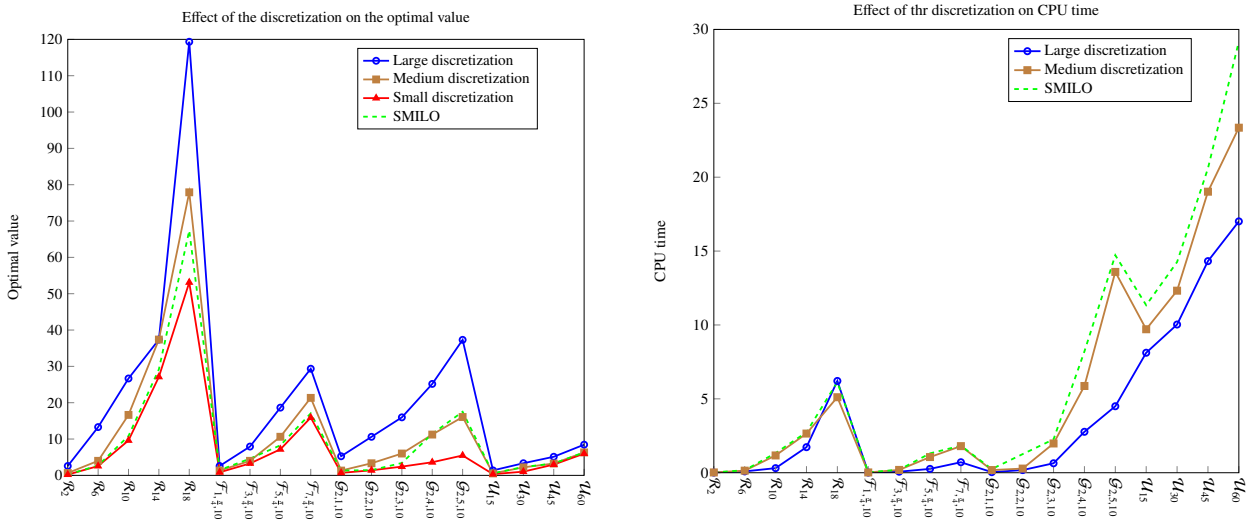

(a) Influence on objective value

(b) Influence on CPU time

Figure 9: Influence of the discretization on the optimal value and the CPU time

CPU time) of the best solution found within a limit of one hour of computations. If the optimal solution is found within one hour, then the resolution stops. Otherwise, we give the value of the best solution found within one hour. Results exhibit very slow resolution times for the classical model. Indeed, only 6 instances out of 24 are solved to optimality within one hour. This observation is a consequence of the fact that the model does not exploit the geometry of the instance: instead of naturally dividing the instance into flight levels, it considers the instance as a whole, hence drastically increasing the complexity of the computations

Table 6: Dimensions of the instances and computational results for the second decomposition method on the multi-level random benchmark

Case	Size		Resolution					
	$\|\mathcal{F}\|$	$\|\mathcal{L}\|$	z_{ip}	*nodes*	t_{ip}	CPLEX Calls	z^f_{best}	t^f_{best}
$\mathcal{M}_{100,10}$	100	10	6.27	0	3.01	20	5.16	2692.44
$\mathcal{M}_{100,12}$	100	12	4.96	0	1.49	24	4.96	2310.54
$\mathcal{M}_{100,14}$	100	14	4.93	0	0.54	28	4.93	2066.45
$\mathcal{M}_{100,16}$	100	16	3.92	0	0.95	32	3.92	1975.94
$\mathcal{M}_{100,18}$	100	18	3.33	0	0.61	36	3.33	1964.45
$\mathcal{M}_{100,20}$	100	20	2.98	0	0.39	40	2.98	1712.24
$\mathcal{M}_{150,10}$	150	10	18.15	0	2.85	20	23.05	3600
$\mathcal{M}_{150,12}$	150	12	12.45	0	2.47	24	19.05	3600
$\mathcal{M}_{150,14}$	150	14	9.67	0	1.16	28	17.03	3600
$\mathcal{M}_{150,16}$	150	16	9.03	0	1.71	32	16.15	3600
$\mathcal{M}_{150,18}$	150	18	7.05	0	0.9	36	12.48	3600
$\mathcal{M}_{150,20}$	150	20	2.68	32	0.62	40	6.12	3600
$\mathcal{M}_{200,10}$	200	10	13.4	35	5.63	20	45.2	3600
$\mathcal{M}_{200,12}$	200	12	12.71	0	4.03	24	31.02	3600
$\mathcal{M}_{200,14}$	200	14	11.97	25	4.42	28	29.45	3600
$\mathcal{M}_{200,16}$	200	16	12.04	0	3.5	32	22.08	3600
$\mathcal{M}_{200,18}$	200	18	8.15	0	1.85	36	18.45	3600
$\mathcal{M}_{200,20}$	200	20	5.36	0	3.3	40	12.45	3600
$\mathcal{M}_{250,10}$	250	10	30.24	234	8.12	20	101.35	3600
$\mathcal{M}_{250,12}$	250	12	24.15	42	8.1	24	80.15	3600
$\mathcal{M}_{250,14}$	250	14	21.45	0	5.12	28	78.11	3600
$\mathcal{M}_{250,16}$	250	16	18.04	0	4	32	64.15	3600
$\mathcal{M}_{250,18}$	250	18	16.41	0	4.26	36	24.48	3600
$\mathcal{M}_{250,20}$	250	20	11.05	0	3.81	40	21.35	3600

to perform. On the contrary, the decomposition method benefits from the geometry of the instances and the weak interdepedency between flight levels to perform a more efficient resolution. As a consequence, every instance is solved to optimality within 9 seconds.

6 Conclusions

In this article, we started by designing an optimization model for the air conflict resolution problem. To this end, we designed a graph whose vertices correspond to maneuvers and whose edges link conflict-free maneuvers of distinct aircraft. A solution to the problem corresponds to a maximum clique of minimum cost in the graph. The cost structure used in the model is specific, since the cost of the vertices depends on the vertices belonging to the maximum clique. This specificity makes the model an original variant of the search for a maximum clique of minimum weight. The main advantage of our model is its flexibility, since the resolution process is fully separated from the modeling of the problem. As a consequence, the mathematical framework remains valid under a large variety of assumptions. This is an interesting feature for the community since in the future we will be able to compare this model to other existing models.

Since the clique search problem is $\mathcal{NP}$-hard, a sensitivity of the solution time regarding the number of maneuvers per aircraft could be expected. Besides, in practice the set of aircraft has weak geometric dependencies that could be taken advantage of. However, these dependencies do not appear explicitly in the model. To address these two observations, we designed two decomposition methods. The first one is a sequential mixed integer linear optimization procedure iteratively solving the problem while changing the discretization. With this method we achieve a trade-off between finding economically efficient solutions while not taking too much time. The second one uses this method as a subroutine of a meta-heuristic exploiting the geometry of the instances by solving local parts of the instances before solving them globally.

We performed tests for our model on structured instances known to be complex. Results exhibit small solution times (less than 15 seconds for instances involving up to 20 aircraft). For larger instances, solution times tend to slightly increase but remain almost real-time. Simulations highlight the sensitivity of the model regarding the number of maneuvers. In this setting, the first decomposition method corresponds to a good trade-off between solution time and cost efficiency. Moreover, it can be considered as an efficient way to solve the problem according to the user's preferences, whether they are more time or cost oriented. The second procedure solved instances with up to 250 aircraft divided between up to 20 flight levels in less than 5 seconds, whereas with the original model the optimal solution could not be found within an hour.

Further research will introduce uncertainties in our model. These uncertainties can be of different types: we can consider errors in the trajectory prediction, or introduce wind to have a more realistic footing for our study. Real-life instances would also be valuable to validate the performance of our model, and in particular instances with aircraft changing altitudes. For such instances, it would be of great interest to adapt the second procedure presented in this article.

A Appendix

A.1 Detailed results for the benchmark without altitude changes

Table 7: Dimensions of the instances and computational results

		Graph $\mathcal{G}$				MILP		Resolution			
Instance type	Case	$\lvert\mathcal{F}\rvert$	$\lvert\mathcal{V}\rvert$	$\lvert\mathcal{E}\rvert$	d	m	n	z_{ip}	$nodes$	t_{lp}	t_{ip}
Roundabout	$\mathcal{R}_2$	2	26	114	0.67	52	283	0.65	0	0.02	0.02
	$\mathcal{R}_4$	4	52	612	0.6	104	1333	2.66	27	0.02	0.07
	$\mathcal{R}_6$	6	78	1526	0.6	156	3215	4	0	0.02	0.14
	$\mathcal{R}_8$	8	104	2744	0.58	208	5705	5.34	75	0.02	0.51
	$\mathcal{R}_{10}$	10	130	4358	0.57	260	8987	16.64	64	0.02	1.17
	$\mathcal{R}_{12}$	12	156	6300	0.56	312	12925	19.99	84	0.02	2.95
	$\mathcal{R}_{14}$	14	182	8608	0.56	364	17595	37.38	0	0.02	2.65
	$\mathcal{R}_{16}$	16	208	11396	0.56	416	23225	42.73	39	0.02	6.99
	$\mathcal{R}_{18}$	18	234	14334	0.55	468	29155	77.91	45	0.02	5.11
	$\mathcal{R}_{20}$	20	260	17756	0.55	520	36053	86.59	71	0.02	11.63
	$\mathcal{F}_{1,15,10}$	2	26	72	0.43	52	199	3.25	0	0.02	0.05
	$\mathcal{F}_{1,30,10}$	2	26	75	0.44	52	205	3.25	34	0.02	0.05
	$\mathcal{F}_{1,45,10}$	2	26	94	0.56	52	243	1.32	0	0.02	0.02
	$\mathcal{F}_{1,60,10}$	2	26	102	0.6	52	259	1.32	0	0.02	0.05
	$\mathcal{F}_{1,75,10}$	2	26	114	0.67	52	283	0.65	0	0.02	0.03
	$\mathcal{F}_{1,90,10}$	2	26	114	0.67	52	283	0.65	0	0.02	0.04
	$\mathcal{F}_{1,105,10}$	2	26	112	0.66	52	279	0.65	0	0.02	0.04
	$\mathcal{F}_{1,120,10}$	2	26	112	0.66	52	279	0.65	0	0.02	0.02
	$\mathcal{F}_{1,135,10}$	2	26	114	0.67	52	283	0.65	0	0.02	0.05
	$\mathcal{F}_{1,150,10}$	2	26	114	0.67	52	283	0.65	0	0.02	0.03
	$\mathcal{F}_{1,165,10}$	2	26	114	0.67	52	283	0.65	0	0.02	0.04
	$\mathcal{F}_{2,15,10}$	4	52	721	0.71	104	1551	6.6	40	0.02	0.09
	$\mathcal{F}_{2,30,10}$	4	52	706	0.7	104	1521	6.6	79	0.02	0.09
	$\mathcal{F}_{2,45,10}$	4	52	724	0.71	104	1557	2.66	0	0.02	0.08
	$\mathcal{F}_{2,60,10}$	4	52	736	0.73	104	1581	2.66	0	0.02	0.06
	$\mathcal{F}_{2,75,10}$	4	52	761	0.75	104	1631	1.99	0	0.02	0.06
	$\mathcal{F}_{2,90,10}$	4	52	772	0.76	104	1653	1.32	57	0.02	0.13
	$\mathcal{F}_{2,105,10}$	4	52	782	0.77	104	1673	1.32	77	0.02	0.14
	$\mathcal{F}_{2,120,10}$	4	52	776	0.77	104	1661	1.32	0	0.02	0.15
	$\mathcal{F}_{2,135,10}$	4	52	754	0.74	104	1617	1.32	0	0.02	0.05
	$\mathcal{F}_{2,150,10}$	4	52	746	0.74	104	1601	1.32	57	0.02	0.15
	$\mathcal{F}_{2,165,10}$	4	52	752	0.74	104	1613	1.32	0	0.02	0.08
	$\mathcal{F}_{3,15,10}$	6	78	2002	0.79	156	4167	9.95	0	0.02	0.16
	$\mathcal{F}_{3,30,10}$	6	78	1967	0.78	156	4097	9.95	155	0.02	0.37
	$\mathcal{F}_{3,45,10}$	6	78	1972	0.78	156	4107	4	0	0.02	0.19
	$\mathcal{F}_{3,60,10}$	6	78	1980	0.78	156	4123	4	0	0.02	0.18
	$\mathcal{F}_{3,75,10}$	6	78	1988	0.78	156	4139	3.33	0	0.02	0.17
	$\mathcal{F}_{3,90,10}$	6	78	1991	0.79	156	4145	2.66	0	0.02	0.17
	$\mathcal{F}_{3,105,10}$	6	78	2023	0.8	156	4209	1.99	0	0.02	0.14
	$\mathcal{F}_{3,120,10}$	6	78	2006	0.79	156	4175	1.99	0	0.02	0.17

Table 7: Dimensions of the instances and computational results (cont.)

		Graph $\mathcal{G}$				MILP		Resolution			
Instance type	Case	$\|\mathcal{F}\|$	$\|\mathcal{V}\|$	$\|\mathcal{E}\|$	d	m	n	z_{ip}	$nodes$	t_{lp}	t_{ip}
	$\mathcal{F}_{3,135,10}$	6	78	1974	0.78	156	4111	2.66	0	0.02	0.16
	$\mathcal{F}_{3,150,10}$	6	78	1916	0.76	156	3995	1.99	0	0.02	0.15
	$\mathcal{F}_{3,165,10}$	6	78	1904	0.75	156	3971	1.99	0	0.02	0.14
	$\mathcal{F}_{4,15,10}$	8	104	3918	0.83	208	8053	13.29	0	0.02	0.37
	$\mathcal{F}_{4,30,10}$	8	104	3855	0.81	208	7927	14.74	167	0.02	0.69
	$\mathcal{F}_{4,45,10}$	8	104	3852	0.81	208	7921	7.27	0	0.02	0.41
	$\mathcal{F}_{4,60,10}$	8	104	3846	0.81	208	7909	5.34	57	0.02	0.57
	$\mathcal{F}_{4,75,10}$	8	104	3834	0.81	208	7885	4.67	0	0.02	0.38
	$\mathcal{F}_{4,90,10}$	8	104	3820	0.81	208	7857	4	0	0.02	0.32
	$\mathcal{F}_{4,105,10}$	8	104	3825	0.81	208	7867	3.33	0	0.02	0.4
	$\mathcal{F}_{4,120,10}$	8	104	3805	0.8	208	7827	2.66	0	0.02	0.27
	$\mathcal{F}_{4,135,10}$	8	104	3747	0.79	208	7711	3.33	0	0.02	0.28
	$\mathcal{F}_{4,150,10}$	8	104	3670	0.78	208	7557	3.33	0	0.02	0.31
	$\mathcal{F}_{4,165,10}$	8	104	3516	0.74	208	7249	2.66	0	0.02	0.27
	$\mathcal{F}_{5,15,10}$	10	130	6466	0.85	260	13203	16.64	115	0.02	0.8
	$\mathcal{F}_{5,30,10}$	10	130	6380	0.84	260	13031	19.45	131	0.02	1.04
	$\mathcal{F}_{5,45,10}$	10	130	6364	0.84	260	12999	10.62	0	0.02	1.06
	$\mathcal{F}_{5,60,10}$	10	130	6349	0.83	260	12969	6.68	0	0.02	0.9
	$\mathcal{F}_{5,75,10}$	10	130	6309	0.83	260	12889	6.01	0	0.02	0.58
	$\mathcal{F}_{5,90,10}$	10	130	6267	0.82	260	12805	5.34	0	0.02	0.66
	$\mathcal{F}_{5,105,10}$	10	130	6236	0.82	260	12743	4.67	0	0.02	0.61
	$\mathcal{F}_{5,120,10}$	10	130	6164	0.81	260	12599	5.26	0	0.02	0.56
	$\mathcal{F}_{5,135,10}$	10	130	6065	0.8	260	12401	4.67	0	0.02	0.54
	$\mathcal{F}_{5,150,10}$	10	130	5953	0.78	260	12177	4	0	0.02	0.58
	$\mathcal{F}_{5,165,10}$	10	130	5658	0.74	260	11587	4.67	66	0.02	0.78
	$\mathcal{F}_{6,15,10}$	12	156	9650	0.87	312	19625	19.99	0	0.02	0.6
	$\mathcal{F}_{6,30,10}$	12	156	9535	0.85	312	19395	25.58	0	0.02	0.94
	$\mathcal{F}_{6,45,10}$	12	156	9512	0.85	312	19349	15.98	61	0.02	2.02
	$\mathcal{F}_{6,60,10}$	12	156	9483	0.85	312	19291	9.96	70	0.02	1.96
	$\mathcal{F}_{6,75,10}$	12	156	9431	0.85	312	19187	7.35	40	0.02	1.54
	$\mathcal{F}_{6,90,10}$	12	156	9349	0.84	312	19023	6.68	39	0.02	1.51
	$\mathcal{F}_{6,105,10}$	12	156	9266	0.83	312	18857	7.27	0	0.02	1.07
	$\mathcal{F}_{6,120,10}$	12	156	9139	0.82	312	18603	6.68	0	0.02	0.84
	$\mathcal{F}_{6,135,10}$	12	156	8936	0.8	312	18197	7.27	44	0.02	1.37
	$\mathcal{F}_{6,150,10}$	12	156	8787	0.79	312	17899	6.01	30	0.02	1.18
	$\mathcal{F}_{6,165,10}$	12	156	8366	0.75	312	17057	6.01	32	0.02	1.44
	$\mathcal{F}_{7,15,10}$	14	182	13472	0.88	364	27323	23.34	0	0.02	0.91
	$\mathcal{F}_{7,30,10}$	14	182	13331	0.87	364	27041	32.31	0	0.02	0.58
	$\mathcal{F}_{7,45,10}$	14	182	13298	0.86	364	26975	21.33	0	0.02	1.8
	$\mathcal{F}_{7,60,10}$	14	182	13252	0.86	364	26883	13.3	0	0.02	1.44
	$\mathcal{F}_{7,75,10}$	14	182	13183	0.86	364	26745	10.63	96	0.02	3
	$\mathcal{F}_{7,90,10}$	14	182	13067	0.85	364	26513	9.96	44	0.02	1.98
	$\mathcal{F}_{7,105,10}$	14	182	12941	0.84	364	26261	8.69	123	0.02	2.83
	$\mathcal{F}_{7,120,10}$	14	182	12750	0.83	364	25879	8.02	0	0.02	1.4
	$\mathcal{F}_{7,135,10}$	14	182	12396	0.81	364	25171	8.69	58	0.02	2.44
	$\mathcal{F}_{7,150,10}$	14	182	12123	0.79	364	24625	8.02	72	0.02	2.41
	$\mathcal{F}_{7,165,10}$	14	182	11588	0.75	364	23555	8.62	46	0.02	2.31
	$\mathcal{F}_{8,15,10}$	16	208	17926	0.88	416	36285	26.68	0	0.02	0.89
	$\mathcal{F}_{8,30,10}$	16	208	17766	0.88	416	35965	42.24	0	0.02	0.59
	$\mathcal{F}_{8,45,10}$	16	208	17717	0.87	416	35867	31.26	0	0.02	0.75
	$\mathcal{F}_{8,60,10}$	16	208	17659	0.87	416	35751	18.66	0	0.02	1.7
	$\mathcal{F}_{8,75,10}$	16	208	17567	0.87	416	35567	15.98	0	0.02	2.32
	$\mathcal{F}_{8,90,10}$	16	208	17422	0.86	416	35277	13.3	30	0.02	3.05
	$\mathcal{F}_{8,105,10}$	16	208	17251	0.85	416	34935	11.96	61	0.02	2.98
	$\mathcal{F}_{8,120,10}$	16	208	16974	0.84	416	34381	12.63	0	0.02	2.98
	$\mathcal{F}_{8,135,10}$	16	208	16453	0.81	416	33339	13.3	80	0.02	4.06
	$\mathcal{F}_{8,150,10}$	16	208	15997	0.79	416	32427	12.7	45	0.02	4.53
	$\mathcal{F}_{8,165,10}$	16	208	15220	0.75	416	30873	11.29	125	0.02	4.19
	$\mathcal{G}_{2,1,10}$	4	52	787	0.78	104	1683	1.32	35	0.02	0.18
	$\mathcal{G}_{2,2,10}$	8	104	3780	0.8	208	7777	3.33	0	0.02	0.28
Grids	$\mathcal{G}_{2,3,10}$	12	156	9072	0.81	312	18469	6.01	29	0.02	1.98
	$\mathcal{G}_{2,4,10}$	16	208	16854	0.83	416	34141	11.23	55	0.02	5.87
	$\mathcal{G}_{2,5,10}$	20	260	27207	0.85	520	54955	16.06	138	0.02	13.59

Table 7: Dimensions of the instances and computational results (cont.)

		Graph $\mathcal{G}$				MILP		Resolution			
Instance type	Case	$\lvert\mathcal{F}\rvert$	$\lvert\mathcal{V}\rvert$	$\lvert\mathcal{E}\rvert$	d	m	n	z_{ip}	$nodes$	t_{lp}	t_{ip}
Random	$\mathcal{U}_5$	5	55	726	1	110	1567	0	0	0.02	0
	$\mathcal{U}_{10}$	10	110	4830	0.99	220	9890	0	0	0.02	0
	$\mathcal{U}_{15}$	15	165	9865	0.99	330	20075	0.32	0	0.02	0.56
	$\mathcal{U}_{20}$	20	220	14365	0.99	440	29190	0.54	8	0.02	1.1
	$\mathcal{U}_{25}$	25	275	19182	0.98	550	38939	2.25	19	0.02	2.1
	$\mathcal{U}_{30}$	30	330	28750	0.99	660	58190	0.21	45	0.02	4.32
	$\mathcal{U}_{35}$	35	385	31406	0.99	770	63617	0.21	75	0.02	6.25
	$\mathcal{U}_{40}$	40	440	52766	0.99	880	106452	0.21	119	0.02	9.63
	$\mathcal{U}_{45}$	45	495	62051	0.99	990	125137	0.86	179	0.02	10.02
	$\mathcal{U}_{50}$	50	550	57215	1	1100	115580	0	225	0.02	10.06
	$\mathcal{U}_{55}$	55	605	69090	0.99	1210	139445	4.83	346	0.02	12.21
	$\mathcal{U}_{60}$	60	660	75338	0.98	1320	152056	0.32	561	0.02	19.35

A.2 Detailed results for the benchmark with altitude changes

Table 8: Dimensions of the instances and computational results

		Graph $\mathcal{G}$				MILP		Resolution			
Instance type	Case	$\lvert\mathcal{F}\rvert$	$\lvert\mathcal{V}\rvert$	$\lvert\mathcal{E}\rvert$	d	m	n	z_{ip}	$nodes$	t_{lp}	t_{ip}
Roundabout	$\mathcal{R}_2$	2	30	168	0.75	60	399	0.65	21	0.02	0.04
	$\mathcal{R}_4$	4	60	936	0.69	120	1997	2.66	0	0.02	0.08
	$\mathcal{R}_6$	6	90	2336	0.69	180	4859	4	99	0.02	0.35
	$\mathcal{R}_8$	8	120	4256	0.68	240	8761	5.34	67	0.02	0.7
	$\mathcal{R}_{10}$	10	150	6788	0.67	300	13887	16.64	0	0.02	1.11
	$\mathcal{R}_{12}$	12	180	9864	0.66	360	20101	19.99	108	0.02	4.27
	$\mathcal{R}_{14}$	14	210	13522	0.66	420	27479	37.38	155	0.02	9.67
	$\mathcal{R}_{16}$	16	240	17876	0.66	480	36249	42.73	96	0.02	16.63
	$\mathcal{R}_{18}$	18	270	22596	0.66	540	45751	77.91	154	0.02	23.8
	$\mathcal{R}_{20}$	20	300	28016	0.66	600	56653	86.59	277	0.02	37.1
	$\mathcal{F}_{1,15,10}$	2	30	126	0.56	60	315	3.25	0	0.02	0.09
	$\mathcal{F}_{1,30,10}$	2	30	129	0.57	60	321	3.25	34	0.02	0.11
	$\mathcal{F}_{1,45,10}$	2	30	148	0.66	60	359	1.32	0	0.02	0.02
	$\mathcal{F}_{1,60,10}$	2	30	156	0.69	60	375	1.32	0	0.02	0.02
	$\mathcal{F}_{1,75,10}$	2	30	168	0.75	60	399	0.65	0	0.02	0.12
	$\mathcal{F}_{1,90,10}$	2	30	168	0.75	60	399	0.65	0	0.02	0.1
	$\mathcal{F}_{1,105,10}$	2	30	166	0.74	60	395	0.65	0	0.02	0.04
	$\mathcal{F}_{1,120,10}$	2	30	166	0.74	60	395	0.65	0	0.02	0.04
	$\mathcal{F}_{1,135,10}$	2	30	168	0.75	60	399	0.65	21	0.02	0.14
	$\mathcal{F}_{1,150,10}$	2	30	168	0.75	60	399	0.65	21	0.02	0.09
	$\mathcal{F}_{1,165,10}$	2	30	168	0.75	60	399	0.65	21	0.02	0.08
	$\mathcal{F}_{2,15,10}$	4	60	1053	0.78	120	2231	6.6	31	0.02	0.19
	$\mathcal{F}_{2,30,10}$	4	60	1038	0.77	120	2201	6.6	84	0.02	0.17
	$\mathcal{F}_{2,45,10}$	4	60	1056	0.78	120	2237	2.66	35	0.02	0.19
	$\mathcal{F}_{2,60,10}$	4	60	1068	0.79	120	2261	2.66	54	0.02	0.22
	$\mathcal{F}_{2,75,10}$	4	60	1093	0.81	120	2311	1.99	49	0.02	0.12
	$\mathcal{F}_{2,90,10}$	4	60	1104	0.82	120	2333	1.32	32	0.02	0.15
	$\mathcal{F}_{2,105,10}$	4	60	1114	0.83	120	2353	1.32	0	0.02	0.1
	$\mathcal{F}_{2,120,10}$	4	60	1108	0.82	120	2341	1.32	64	0.02	0.23
	$\mathcal{F}_{2,135,10}$	4	60	1082	0.8	120	2289	1.32	0	0.02	0.1
	$\mathcal{F}_{2,150,10}$	4	60	1074	0.8	120	2273	1.32	62	0.02	0.17
	$\mathcal{F}_{2,165,10}$	4	60	1080	0.8	120	2285	1.32	62	0.02	0.16
	$\mathcal{F}_{3,15,10}$	6	90	2836	0.84	180	5859	9.95	79	0.02	0.52
	$\mathcal{F}_{3,30,10}$	6	90	2801	0.83	180	5789	9.95	123	0.02	0.55
	$\mathcal{F}_{3,45,10}$	6	90	2806	0.83	180	5799	4	0	0.02	0.27
	$\mathcal{F}_{3,60,10}$	6	90	2814	0.83	180	5815	4	0	0.02	0.23
	$\mathcal{F}_{3,75,10}$	6	90	2822	0.84	180	5831	3.33	0	0.02	0.17
	$\mathcal{F}_{3,90,10}$	6	90	2825	0.84	180	5837	2.66	0	0.02	0.23
	$\mathcal{F}_{3,105,10}$	6	90	2857	0.85	180	5901	1.99	0	0.02	0.24
	$\mathcal{F}_{3,120,10}$	6	90	2840	0.84	180	5867	1.99	0	0.02	0.23
	$\mathcal{F}_{3,135,10}$	6	90	2800	0.83	180	5787	2.66	0	0.02	0.21

Table 8: Dimensions of the instances and computational results (cont.)

		Graph $\mathcal{G}$				MILP		Resolution			
Instance type	Case	$\|\mathcal{F}\|$	$\|\mathcal{V}\|$	$\|\mathcal{E}\|$	d	m	n	z_{ip}	$nodes$	t_{lp}	t_{ip}
	$\mathcal{F}_{3,150,10}$	6	90	2742	0.81	180	5671	1.99	0	0.02	0.21
	$\mathcal{F}_{3,165,10}$	6	90	2726	0.81	180	5639	1.99	0	0.02	0.26
	$\mathcal{F}_{4,15,10}$	8	120	5478	0.87	240	11205	13.29	90	0.02	0.97
	$\mathcal{F}_{4,30,10}$	8	120	5415	0.86	240	11079	14.74	170	0.02	1.03
	$\mathcal{F}_{4,45,10}$	8	120	5412	0.86	240	11073	7.27	0	0.02	0.56
	$\mathcal{F}_{4,60,10}$	8	120	5406	0.86	240	11061	5.34	75	0.02	0.98
	$\mathcal{F}_{4,75,10}$	8	120	5394	0.86	240	11037	4.67	0	0.02	0.55
	$\mathcal{F}_{4,90,10}$	8	120	5380	0.85	240	11009	4	0	0.02	0.52
	$\mathcal{F}_{4,105,10}$	8	120	5385	0.85	240	11019	3.33	0	0.02	0.44
	$\mathcal{F}_{4,120,10}$	8	120	5365	0.85	240	10979	2.66	0	0.02	0.45
	$\mathcal{F}_{4,135,10}$	8	120	5295	0.84	240	10839	3.33	0	0.02	0.47
	$\mathcal{F}_{4,150,10}$	8	120	5218	0.83	240	10685	3.33	0	0.02	0.49
	$\mathcal{F}_{4,165,10}$	8	120	5052	0.8	240	10353	2.66	0	0.02	0.52
	$\mathcal{F}_{5,15,10}$	10	150	8976	0.89	300	18263	16.64	54	0.02	2.01
	$\mathcal{F}_{5,30,10}$	10	150	8890	0.88	300	18091	19.45	135	0.02	1.98
	$\mathcal{F}_{5,45,10}$	10	150	8874	0.88	300	18059	10.62	86	0.02	1.92
	$\mathcal{F}_{5,60,10}$	10	150	8859	0.87	300	18029	6.68	0	0.02	1.19
	$\mathcal{F}_{5,75,10}$	10	150	8819	0.87	300	17949	6.01	77	0.02	1.69
	$\mathcal{F}_{5,90,10}$	10	150	8777	0.87	300	17865	5.34	79	0.02	1.56
	$\mathcal{F}_{5,105,10}$	10	150	8746	0.86	300	17803	4.67	65	0.02	1.51
	$\mathcal{F}_{5,120,10}$	10	150	8674	0.86	300	17659	5.26	77	0.02	1.6
	$\mathcal{F}_{5,135,10}$	10	150	8559	0.85	300	17429	4.67	0	0.02	1.02
	$\mathcal{F}_{5,150,10}$	10	150	8447	0.83	300	17205	4	0	0.02	0.92
	$\mathcal{F}_{5,165,10}$	10	150	8132	0.8	300	16575	4.67	0	0.02	0.75
	$\mathcal{F}_{6,15,10}$	12	180	13334	0.9	360	27041	19.99	175	0.02	2.86
	$\mathcal{F}_{6,30,10}$	12	180	13219	0.89	360	26811	25.58	149	0.02	3.06
	$\mathcal{F}_{6,45,10}$	12	180	13196	0.89	360	26765	15.98	143	0.02	3.4
	$\mathcal{F}_{6,60,10}$	12	180	13167	0.89	360	26707	9.96	74	0.02	2.4
	$\mathcal{F}_{6,75,10}$	12	180	13115	0.88	360	26603	7.35	55	0.02	2.44
	$\mathcal{F}_{6,90,10}$	12	180	13033	0.88	360	26439	6.68	116	0.02	2.33
	$\mathcal{F}_{6,105,10}$	12	180	12950	0.87	360	26273	7.27	75	0.02	2.76
	$\mathcal{F}_{6,120,10}$	12	180	12823	0.86	360	26019	6.68	88	0.02	2.62
	$\mathcal{F}_{6,135,10}$	12	180	12600	0.85	360	25573	7.27	0	0.02	2.55
	$\mathcal{F}_{6,150,10}$	12	180	12451	0.84	360	25275	6.01	0	0.02	1.88
	$\mathcal{F}_{6,165,10}$	12	180	12002	0.81	360	24377	6.01	0	0.02	2.16
	$\mathcal{F}_{7,15,10}$	14	210	18554	0.91	420	37543	23.34	159	0.02	3.72
	$\mathcal{F}_{7,30,10}$	14	210	18413	0.9	420	37261	32.31	334	0.02	5.88
	$\mathcal{F}_{7,45,10}$	14	210	18380	0.9	420	37195	21.33	164	0.02	3.94
	$\mathcal{F}_{7,60,10}$	14	210	18334	0.9	420	37103	13.3	123	0.02	3.6
	$\mathcal{F}_{7,75,10}$	14	210	18265	0.89	420	36965	10.63	115	0.02	3.77
	$\mathcal{F}_{7,90,10}$	14	210	18149	0.89	420	36733	9.96	48	0.02	2.55
	$\mathcal{F}_{7,105,10}$	14	210	18023	0.88	420	36481	8.69	133	0.02	3.05
	$\mathcal{F}_{7,120,10}$	14	210	17832	0.87	420	36099	8.02	69	0.02	2.95
	$\mathcal{F}_{7,135,10}$	14	210	17454	0.85	420	35343	8.69	160	0.02	4.79
	$\mathcal{F}_{7,150,10}$	14	210	17181	0.84	420	34797	8.02	114	0.02	3.51
	$\mathcal{F}_{7,165,10}$	14	210	16610	0.81	420	33655	8.62	68	0.02	4.67
	$\mathcal{F}_{8,15,10}$	16	240	24630	0.91	480	49757	26.68	118	0.02	6.92
	$\mathcal{F}_{8,30,10}$	16	240	24470	0.91	480	49437	42.24	160	0.02	7.57
	$\mathcal{F}_{8,45,10}$	16	240	24421	0.9	480	49339	31.26	213	0.02	7.69
	$\mathcal{F}_{8,60,10}$	16	240	24363	0.9	480	49223	18.66	103	0.02	7.2
	$\mathcal{F}_{8,75,10}$	16	240	24271	0.9	480	49039	15.98	129	0.02	6.91
	$\mathcal{F}_{8,90,10}$	16	240	24126	0.89	480	48749	13.3	106	0.02	7.43
	$\mathcal{F}_{8,105,10}$	16	240	23955	0.89	480	48407	11.96	252	0.02	8.62
	$\mathcal{F}_{8,120,10}$	16	240	23678	0.88	480	47853	12.63	160	0.02	9.78
	$\mathcal{F}_{8,135,10}$	16	240	23129	0.86	480	46755	13.3	122	0.02	7.65
	$\mathcal{F}_{8,150,10}$	16	240	22673	0.84	480	45843	12.7	70	0.02	7.05
	$\mathcal{F}_{8,165,10}$	16	240	21852	0.81	480	44201	11.29	57	0.02	7.18
	$\mathcal{F}_{9,15,10}$	18	270	31506	0.92	540	63571	30.03	53	0.02	8.35
	$\mathcal{F}_{9,30,10}$	18	270	31387	0.91	540	63333	53.88	240	0.02	10.68
	$\mathcal{F}_{9,45,10}$	18	270	31335	0.91	540	63229	42.9	177	0.02	9.91
	$\mathcal{F}_{9,60,10}$	18	270	31261	0.91	540	63081	30.18	79	0.02	9.13
	$\mathcal{F}_{9,75,10}$	18	270	31143	0.9	540	62845	24.66	103	0.02	12.08
	$\mathcal{F}_{9,90,10}$	18	270	30966	0.9	540	62491	21.87	160	0.02	12.34
	$\mathcal{F}_{9,105,10}$	18	270	30755	0.89	540	62069	18.52	122	0.02	11.83

Table 8: Dimensions of the instances and computational results (cont.)

Instance type	Case	Graph $\mathcal{G}$				MILP		Resolution			
		$\lvert\mathcal{F}\rvert$	$\lvert\mathcal{V}\rvert$	$\lvert\mathcal{E}\rvert$	d	m	n	z_{ip}	$nodes$	t_{lp}	t_{ip}
	$\mathcal{F}_{9,120,10}$	18	270	30384	0.88	540	61327	17.98	169	0.02	10.83
	$\mathcal{F}_{9,135,10}$	18	270	29673	0.86	540	59905	19.85	124	0.02	13.55
	$\mathcal{F}_{9,150,10}$	18	270	28921	0.84	540	58401	20.52	184	0.02	11.77
	$\mathcal{F}_{9,165,10}$	18	270	27688	0.8	540	55935	15.98	77	0.02	11.37
	$\mathcal{F}_{10,15,10}$	20	300	39222	0.92	600	79065	41.55	104	0.02	12.32
	$\mathcal{F}_{10,30,10}$	20	300	39163	0.92	600	78947	65.31	251	0.02	14.19
	$\mathcal{F}_{10,45,10}$	20	300	39111	0.91	600	78843	54.33	168	0.02	14.18
	$\mathcal{F}_{10,60,10}$	20	300	39036	0.91	600	78693	41.61	92	0.02	11.51
	$\mathcal{F}_{10,75,10}$	20	300	38908	0.91	600	78437	36.19	166	0.02	11.87
	$\mathcal{F}_{10,90,10}$	20	300	38697	0.91	600	78015	33.51	74	0.02	10.02
	$\mathcal{F}_{10,105,10}$	20	300	38439	0.9	600	77499	30.16	128	0.02	12.18
	$\mathcal{F}_{10,120,10}$	20	300	37985	0.89	600	76591	29.51	84	0.02	9.95
	$\mathcal{F}_{10,135,10}$	20	300	37103	0.87	600	74827	31.5	78	0.02	10.95
	$\mathcal{F}_{10,150,10}$	20	300	36066	0.84	600	72753	33.23	73	0.02	12.14
	$\mathcal{F}_{10,165,10}$	20	300	34142	0.8	600	68905	30.23	20	0.02	7.93
Grids	$\mathcal{G}_{2,1,10}$	4	60	1115	0.83	120	2355	1.32	53	0.02	0.1
	$\mathcal{G}_{2,2,10}$	8	120	5332	0.85	240	10913	3.33	0	0.02	0.42
	$\mathcal{G}_{2,3,10}$	12	180	12744	0.86	360	25861	6.01	0	0.02	2.01
	$\mathcal{G}_{2,4,10}$	16	240	23542	0.87	480	47581	11.23	185	0.02	10.05
Random	$\mathcal{U}_5$	5	75	1209	1	150	2573	0.01	0	0.02	0.01
	$\mathcal{U}_{10}$	10	150	4839	1	300	9988	0.01	0	0.02	0.07
	$\mathcal{U}_{15}$	15	225	8939	0.98	450	18343	0.86	0	0.02	1.25
	$\mathcal{U}_{20}$	20	300	16732	0.99	600	34084	0.97	0	0.02	2.55
	$\mathcal{U}_{25}$	25	375	22345	0.98	750	45465	1.29	38	0.02	3.55
	$\mathcal{U}_{30}$	30	450	32248	0.99	900	65426	1.37	31	0.02	6.46
	$\mathcal{U}_{35}$	35	525	42027	0.99	1050	85139	1.76	0	0.02	11.22
	$\mathcal{U}_{40}$	40	600	50386	0.99	1200	102012	2.04	0	0.02	20.15
	$\mathcal{U}_{45}$	45	675	60764	0.99	1350	122923	1.18	41	0.02	24.02
	$\mathcal{U}_{50}$	50	750	69035	0.99	1500	139620	2.12	0	0.02	27.47
	$\mathcal{U}_{55}$	55	825	84344	0.99	1650	170393	3.55	89	0.02	40.16
	$\mathcal{U}_{60}$	60	900	75126	0.99	1800	152112	4.54	26	0.02	55.25

A.3 Detailed reports on the influence of discretization on the objective value and the CPU time and comparison with the SMILO procedure results

Table 9: Dimensions of the instances and computational results

Instance type	Case	Large discretization		Medium discretization		Small disctretization		Iterative procedure		
		z_{ip}	t_{ip}	z_{ip}	t_{ip}	z_{ip}	t_{ip}	z_{ip}	t_{ip}	CPLEX Calls
Roundabout	$\mathcal{R}_2$	2.58	0.01	0.65	0.02	0.21	0.27	0.21	0.02	4
	$\mathcal{R}_4$	7.93	0.04	2.66	0.07	0.96	1.45	1.06	0.06	4
	$\mathcal{R}_6$	13.29	0.09	4	0.14	2.56	5.62	2.73	0.12	4
	$\mathcal{R}_8$	18.64	0.25	5.34	0.51	5.34	69.2	6.42	0.26	4
	$\mathcal{R}_{10}$	26.67	0.31	16.64	1.17	9.62	244.39	10.84	0.33	3
	$\mathcal{R}_{12}$	32.03	0.72	19.99	2.95	15.71	362.06	18.03	0.75	3
	$\mathcal{R}_{14}$	37.38	1.73	37.38	2.65	27.11	1382.58	29.19	1.74	3
	$\mathcal{R}_{16}$	42.73	2.37	42.73	6.99	38.67	2414.48	42.73	2.41	3
	$\mathcal{R}_{18}$	119.34	6.21	77.91	5.11	53.11	1316.5	67.38	6.14	4
	$\mathcal{R}_{20}$	132.65	10.59	86.59	11.63	76.56	1162.29	86.59	10.39	4
	$\mathcal{F}_{1,15,10}$	5.26	0.02	3.25	0.05	2.97	0.39	2.96	0.03	3
	$\mathcal{F}_{1,30,10}$	5.26	0.01	3.25	0.05	1.9	0.33	2.12	0.02	3
	$\mathcal{F}_{1,45,10}$	2.58	0.01	1.32	0.02	0.84	0.35	1.46	0.01	4
	$\mathcal{F}_{1,60,10}$	2.58	0.01	1.32	0.05	0.47	0.45	0.67	0.02	3
	$\mathcal{F}_{1,75,10}$	2.58	0.02	0.65	0.03	0.34	0.38	0.38	0.02	5
	$\mathcal{F}_{1,90,10}$	2.58	0.01	0.65	0.04	0.34	0.28	0.27	0.01	3
	$\mathcal{F}_{1,105,10}$	2.58	0.02	0.65	0.04	0.21	0.29	0.21	0.02	4
	$\mathcal{F}_{1,120,10}$	2.58	0.01	0.65	0.02	0.21	0.48	0.19	0.03	3

Table 9: Dimensions of the instances and computational results (cont.)

Instance type	Case	Large discretization		Medium discretization		Small disctretization		Iterative procedure		
		z_{ip}	t_{ip}	z_{ip}	t_{ip}	z_{ip}	t_{ip}	z_{ip}	t_{ip}	CPLEX Calls
	$\mathcal{F}_{1,135,10}$	2.58	0.01	0.65	0.05	0.21	0.4	0.19	0.02	3
	$\mathcal{F}_{1,150,10}$	2.58	0.01	0.65	0.03	0.13	0.31	0.13	0.02	4
	$\mathcal{F}_{1,165,10}$	2.58	0.01	0.65	0.04	0.13	0.26	0.13	0.03	4
	$\mathcal{F}_{2,15,10}$	10.61	0.03	6.6	0.09	5.99	1.63	5.98	0.04	3
	$\mathcal{F}_{2,30,10}$	10.61	0.03	6.6	0.09	4.16	2.75	4.06	0.04	4
	$\mathcal{F}_{2,45,10}$	5.26	0.03	2.66	0.08	1.93	1.93	2.4	0.05	5
	$\mathcal{F}_{2,60,10}$	5.26	0.03	2.66	0.06	1.14	1.27	4.09	0.04	3
	$\mathcal{F}_{2,75,10}$	5.26	0.03	1.99	0.06	0.82	1.35	1.11	0.05	5
	$\mathcal{F}_{2,90,10}$	5.26	0.03	1.32	0.13	0.69	1.6	1.45	0.05	4
	$\mathcal{F}_{2,105,10}$	5.26	0.04	1.32	0.14	0.43	1.64	1.08	0.06	4
	$\mathcal{F}_{2,120,10}$	5.26	0.06	1.32	0.15	0.43	1.82	0.87	0.08	4
	$\mathcal{F}_{2,135,10}$	5.26	0.05	1.32	0.05	0.47	1.42	0.86	0.06	4
	$\mathcal{F}_{2,150,10}$	5.26	0.04	1.32	0.15	0.39	1.62	0.55	0.05	5
	$\mathcal{F}_{2,165,10}$	5.26	0.03	1.32	0.08	0.35	1.69	0.31	0.08	5
	$\mathcal{F}_{3,15,10}$	15.97	0.08	9.95	0.16	9.02	6.65	8.99	0.09	3
	$\mathcal{F}_{3,30,10}$	15.97	0.09	9.95	0.37	6.79	22.72	7.08	0.11	4
	$\mathcal{F}_{3,45,10}$	7.93	0.07	4	0.19	3.28	13.55	4.61	0.1	4
	$\mathcal{F}_{3,60,10}$	7.93	0.08	4	0.18	2	9.33	2.32	0.11	4
	$\mathcal{F}_{3,75,10}$	7.93	0.08	3.33	0.17	1.31	6.36	2.99	0.12	4
	$\mathcal{F}_{3,90,10}$	7.93	0.08	2.66	0.17	1.17	7.78	2.4	0.11	3
	$\mathcal{F}_{3,105,10}$	7.93	0.09	1.99	0.14	0.77	5.65	1.37	0.13	5
	$\mathcal{F}_{3,120,10}$	7.93	0.08	1.99	0.17	0.82	4.25	1.04	0.14	5
	$\mathcal{F}_{3,135,10}$	7.93	0.07	2.66	0.16	0.75	5.45	3.75	0.1	4
	$\mathcal{F}_{3,150,10}$	7.93	0.07	1.99	0.15	0.66	5.31	1.46	0.11	5
	$\mathcal{F}_{3,165,10}$	7.93	0.07	1.99	0.14	0.61	5.26	0.74	0.12	6
	$\mathcal{F}_{4,15,10}$	21.32	0.17	13.29	0.37	12.05	31.81	12.01	0.19	3
	$\mathcal{F}_{4,30,10}$	21.32	0.19	14.74	0.69	10.2	202.93	11.22	0.22	4
	$\mathcal{F}_{4,45,10}$	13.29	0.26	7.27	0.41	4.9	91.8	6.45	0.26	4
	$\mathcal{F}_{4,60,10}$	10.61	0.17	5.34	0.57	3.09	48.51	7.53	0.19	4
	$\mathcal{F}_{4,75,10}$	10.61	0.13	4.67	0.38	1.97	31.27	4.22	0.18	4
	$\mathcal{F}_{4,90,10}$	10.61	0.16	4	0.32	1.65	31.62	4.44	0.23	4
	$\mathcal{F}_{4,105,10}$	10.61	0.16	3.33	0.4	1.25	26.18	2.59	0.23	5
	$\mathcal{F}_{4,120,10}$	10.61	0.15	2.66	0.27	1.17	17.33	2.72	0.22	4
	$\mathcal{F}_{4,135,10}$	10.61	0.15	3.33	0.28	1.19	17.26	4.62	0.17	4
	$\mathcal{F}_{4,150,10}$	10.61	0.15	3.33	0.31	1.09	15.3	1.5	0.21	5
	$\mathcal{F}_{4,165,10}$	10.61	0.14	2.66	0.27	1.17	14.63	2.92	0.19	4
	$\mathcal{F}_{5,15,10}$	26.67	0.22	16.64	0.8	15.08	21.54	15.02	0.25	3
	$\mathcal{F}_{5,30,10}$	26.67	0.47	19.45	1.04	14.96	354.48	16.57	0.49	4
	$\mathcal{F}_{5,45,10}$	18.64	0.26	10.62	1.06	7.17	723.12	8.27	0.31	4
	$\mathcal{F}_{5,60,10}$	13.29	0.43	6.68	0.9	4.43	157.62	9.22	0.54	4
	$\mathcal{F}_{5,75,10}$	13.29	0.28	6.01	0.58	2.83	88.48	5.71	0.39	4
	$\mathcal{F}_{5,90,10}$	13.29	0.26	5.34	0.66	2.32	63.52	4.32	0.33	3
	$\mathcal{F}_{5,105,10}$	13.29	0.28	4.67	0.61	1.74	25.8	2.84	0.37	5
	$\mathcal{F}_{5,120,10}$	13.29	0.25	5.26	0.56	1.85	40.04	5.72	0.37	5
	$\mathcal{F}_{5,135,10}$	13.29	0.23	4.67	0.54	1.94	31.96	4.28	0.32	4
	$\mathcal{F}_{5,150,10}$	13.29	0.24	4	0.58	1.57	48.03	2.15	0.35	5
	$\mathcal{F}_{5,165,10}$	13.29	0.24	4.67	0.78	1.63	35.91	2.88	0.32	6
	$\mathcal{F}_{6,15,10}$	32.03	0.3	19.99	0.6	18.11	57.2	18.03	0.36	3
	$\mathcal{F}_{6,30,10}$	33.11	0.77	25.58	0.94	20.3	299.33	33.11	0.78	3
	$\mathcal{F}_{6,45,10}$	24	0.76	15.98	2.02	10.58	2766.06	12.74	0.83	4
	$\mathcal{F}_{6,60,10}$	18.64	0.82	9.96	1.96	6.35	681.09	12.39	0.82	3
	$\mathcal{F}_{6,75,10}$	15.97	0.61	7.35	1.54	4.16	289.3	9.41	0.62	4
	$\mathcal{F}_{6,90,10}$	15.97	0.73	6.68	1.51	3.41	264.43	7.43	0.87	5
	$\mathcal{F}_{6,105,10}$	15.97	0.64	7.27	1.07	2.59	49.3	8.89	0.76	5
	$\mathcal{F}_{6,120,10}$	15.97	0.37	6.68	0.84	2.59	98.16	5.12	0.49	4
	$\mathcal{F}_{6,135,10}$	18.64	0.37	7.27	1.37	2.71	74.84	5.82	0.55	5
	$\mathcal{F}_{6,150,10}$	15.97	0.5	6.01	1.18	2.39	65.74	4.74	0.66	5
	$\mathcal{F}_{6,165,10}$	15.97	0.32	6.01	1.44	2.43	65.94	5.4	0.49	6
	$\mathcal{F}_{7,15,10}$	37.38	0.52	23.34	0.91	21.13	46.26	21.05	0.61	3
	$\mathcal{F}_{7,30,10}$	41.52	0.53	32.31	0.58	26.97	287.26	41.52	0.53	3
	$\mathcal{F}_{7,45,10}$	29.35	0.71	21.33	1.8	15.9	1795.26	17.07	0.83	4
	$\mathcal{F}_{7,60,10}$	24	0.9	13.3	1.44	9.35	2431.05	14.45	0.95	4

Table 9: Dimensions of the instances and computational results (cont.)

Instance type	Case	Large discretization		Medium discretization		Small disctretization		Iterative procedure		
		z_{ip}	t_{ip}	z_{ip}	t_{ip}	z_{ip}	t_{ip}	z_{ip}	t_{ip}	CPLEX Calls
	$\mathcal{F}_{7,75,10}$	21.32	0.57	10.63	3	6.08	1175.07	13.17	0.65	4
	$\mathcal{F}_{7,90,10}$	21.32	0.67	9.96	1.98	5.04	852.42	11.3	0.81	5
	$\mathcal{F}_{7,105,10}$	18.64	1.03	8.69	2.83	3.92	244.47	7.19	1.17	4
	$\mathcal{F}_{7,120,10}$	18.64	0.86	8.02	1.4	3.77	294.49	7.23	1.14	5
	$\mathcal{F}_{7,135,10}$	21.32	0.89	8.69	2.44	3.68	261.4	9.62	1.01	5
	$\mathcal{F}_{7,150,10}$	21.32	0.49	8.02	2.41	3.76	264.72	5.74	0.67	5
	$\mathcal{F}_{7,165,10}$	18.64	0.51	8.62	2.31	4.03	148.47	6.16	0.65	4
	$\mathcal{F}_{8,15,10}$	42.73	0.61	26.68	0.89	24.16	51.64	24.06	0.7	3
	$\mathcal{F}_{8,30,10}$	51.99	0.38	42.24	0.59	36.9	134.63	51.99	0.4	3
	$\mathcal{F}_{8,45,10}$	42.37	0.76	31.26	0.75	25.28	1404.96	29.94	0.81	4
	$\mathcal{F}_{8,60,10}$	29.35	0.77	18.66	1.7	14.67	3600.25	17.01	0.82	4
	$\mathcal{F}_{8,75,10}$	26.67	0.78	15.98	2.32	9.72	1352.24	13	0.93	5
	$\mathcal{F}_{8,90,10}$	26.67	1.24	13.3	3.05	7.65	1719.89	12.65	1.4	5
	$\mathcal{F}_{8,105,10}$	24	1.46	11.96	2.98	6.17	356.4	12.77	1.83	4
	$\mathcal{F}_{8,120,10}$	24	0.79	12.63	2.98	5.95	600.42	12.57	0.98	5
	$\mathcal{F}_{8,135,10}$	26.67	1.55	13.3	4.06	5.99	480.72	12.43	1.74	5
	$\mathcal{F}_{9,150,10}$	26.67	1.08	12.7	4.53	5.7	446.92	8.59	1.34	5
	$\mathcal{F}_{8,165,10}$	24	1.19	11.29	4.19	6.39	747.68	9.76	1.43	5
	$\mathcal{G}_{2,1,10}$	5.26	0.04	1.32	0.18	0.69	1.95	1.32	0.05	3
	$\mathcal{G}_{2,2,10}$	10.61	0.18	3.33	0.28	1.39	14.93	1.44	0.26	4
Grids	$\mathcal{G}_{2,3,10}$	15.97	0.64	6.01	1.98	2.41	62.33	3.41	0.96	6
	$\mathcal{G}_{2,4,10}$	25.17	2.77	11.23	5.87	3.61	317.8	11.14	3.21	3
	$\mathcal{G}_{2,5,10}$	37.3	4.5	16.06	13.59	5.48	1845.36	17.51	4.72	5

A.4 Detailed results for the spatial decomposition method applied to the multilevel benchmark

Table 10: Dimensions of the instances and computational results

Case	Size		Resolution					
	$\|\mathcal{F}\|$	$\|\mathcal{L}\|$	z_{ip}	*nodes*	t_{ip}	C-PLEX Calls	z^f_{best}	t^f_{best}
$\mathcal{M}_{100,10}$	100	10	6.27	0	3.01	20	5.16	2692.44
$\mathcal{M}_{100,12}$	100	12	4.96	0	1.49	24	4.96	2310.54
$\mathcal{M}_{100,14}$	100	14	4.93	0	0.54	28	4.93	2066.45
$\mathcal{M}_{100,16}$	100	16	3.92	0	0.95	32	3.92	1975.94
$\mathcal{M}_{100,18}$	100	18	3.33	0	0.61	36	3.33	1964.45
$\mathcal{M}_{100,20}$	100	20	2.98	0	0.39	40	2.98	1712.24
$\mathcal{M}_{110,10}$	110	10	7.45	0	1.94	20	7.45	2754.12
$\mathcal{M}_{110,12}$	110	12	4.02	13	1.31	24	4.02	2675.99
$\mathcal{M}_{110,14}$	110	14	3.15	0	0.37	28	3.15	2457.12
$\mathcal{M}_{110,16}$	110	16	3.04	0	1	32	3.04	2397.06
$\mathcal{M}_{110,18}$	110	18	2.98	0	0.92	36	2.98	2314.15
$\mathcal{M}_{110,20}$	110	20	2.96	0	0.58	40	2.96	2276.14
$\mathcal{M}_{120,10}$	120	10	12.73	85	2.45	20	12.73	3175.97
$\mathcal{M}_{120,12}$	120	12	9.75	7	1.29	24	9.75	3003.46
$\mathcal{M}_{120,14}$	120	14	8.96	0	1.34	28	8.96	2997.03
$\mathcal{M}_{120,16}$	120	16	7.54	0	0.75	32	7.54	2764.08
$\mathcal{M}_{120,18}$	120	18	5.32	13	1.2	36	5.32	2647.16
$\mathcal{M}_{120,20}$	120	20	3.49	0	0.39	40	3.49	2541.79
$\mathcal{M}_{130,10}$	130	10	13.16	33	2.85	20	13.16	3345.1
$\mathcal{M}_{130,12}$	130	12	11.05	0	1.75	24	11.05	3164.45
$\mathcal{M}_{130,14}$	130	14	9.54	0	1.52	28	9.54	3075.13
$\mathcal{M}_{130,16}$	130	16	4.02	83	1.3	32	4.02	2943.47
$\mathcal{M}_{130,18}$	130	18	3.48	0	0.83	36	3.48	2648.21
$\mathcal{M}_{130,20}$	130	20	3.12	0	0.83	40	3.12	2600.15
$\mathcal{M}_{140,10}$	140	10	17.15	126	3.44	20	18.43	3584.12
$\mathcal{M}_{140,12}$	140	12	12.64	0	1.55	24	13.05	3345.15

Table 10: Dimensions of the instances and computational results (cont.)

Case	Size		Resolution					
	$\|\mathcal{F}\|$	$\|\mathcal{L}\|$	z_{ip}	*nodes*	t_{ip}	C-PLEX Calls	z^f_{best}	t^f_{best}
$\mathcal{M}_{140,14}$	140	14	7.54	0	2.35	28	7.54	3100.88
$\mathcal{M}_{140,16}$	140	16	9.35	0	1.48	32	9.35	2975.12
$\mathcal{M}_{140,18}$	140	18	7.45	20	1.48	36	7.45	2803.97
$\mathcal{M}_{140,20}$	140	20	3.02	0	0.5	40	3.02	2746.21
$\mathcal{M}_{150,10}$	150	10	18.15	0	2.85	20	23.05	3600
$\mathcal{M}_{150,12}$	150	12	12.45	0	2.47	24	19.05	3600
$\mathcal{M}_{150,14}$	150	14	9.67	0	1.16	28	17.03	3600
$\mathcal{M}_{150,16}$	150	16	9.03	0	1.71	32	16.15	3600
$\mathcal{M}_{150,18}$	150	18	7.05	0	0.9	36	12.48	3600
$\mathcal{M}_{150,20}$	150	20	2.68	32	0.62	40	6.12	3600
$\mathcal{M}_{160,10}$	160	10	19.85	0	3.2	20	33.78	3600
$\mathcal{M}_{160,12}$	160	12	13.54	39	2.22	24	30.25	3600
$\mathcal{M}_{160,14}$	160	14	11.02	0	2.18	28	24.66	3600
$\mathcal{M}_{160,16}$	160	16	8.16	0	2.05	32	18.47	3600
$\mathcal{M}_{160,18}$	160	18	6.12	61	2.03	36	14.23	3600
$\mathcal{M}_{160,20}$	160	20	4.32	0	0.33	40	9.26	3600
$\mathcal{M}_{170,10}$	170	10	18.22	39	4.43	20	33.15	3600
$\mathcal{M}_{170,12}$	170	12	10.02	57	4.02	24	22.05	3600
$\mathcal{M}_{170,14}$	170	14	8.45	0	2.19	28	18.06	3600
$\mathcal{M}_{170,16}$	170	16	8.02	0	2.45	32	14.06	3600
$\mathcal{M}_{170,18}$	170	18	6.03	0	1.91	36	9.25	3600
$\mathcal{M}_{170,20}$	170	20	5.36	0	1.72	40	10.02	3600
$\mathcal{M}_{180,10}$	180	10	22.02	62	4.13	20	45.03	3600
$\mathcal{M}_{180,12}$	180	12	14.36	0	3.43	24	27.06	3600
$\mathcal{M}_{180,14}$	180	14	12.15	0	2.96	28	18.16	3600
$\mathcal{M}_{180,16}$	180	16	7.15	63	2.49	32	24.02	3600
$\mathcal{M}_{180,18}$	180	18	6.7	0	2.26	36	16.15	3600
$\mathcal{M}_{180,20}$	180	20	6.81	0	1.25	40	14.05	3600
$\mathcal{M}_{190,10}$	190	10	21.54	0	4.31	20	42.05	3600
$\mathcal{M}_{190,12}$	190	12	20.54	0	3.09	24	30.46	3600
$\mathcal{M}_{190,14}$	190	14	20.1	0	3.01	28	29.45	3600
$\mathcal{M}_{190,16}$	190	16	16.09	0	3.92	32	24.59	3600
$\mathcal{M}_{190,18}$	190	18	12.02	0	2.55	36	20.45	3600
$\mathcal{M}_{190,20}$	190	20	8.02	0	2.58	40	18.03	3600
$\mathcal{M}_{200,10}$	200	10	13.4	35	5.63	20	45.2	3600
$\mathcal{M}_{200,12}$	200	12	12.71	0	4.03	24	31.02	3600
$\mathcal{M}_{200,14}$	200	14	11.97	25	4.42	28	29.45	3600
$\mathcal{M}_{200,16}$	200	16	12.04	0	3.5	32	22.08	3600
$\mathcal{M}_{200,18}$	200	18	8.15	0	1.85	36	18.45	3600
$\mathcal{M}_{200,20}$	200	20	5.36	0	3.3	40	12.45	3600
$\mathcal{M}_{210,10}$	210	10	21.69	31	4.42	20	66.1	3600
$\mathcal{M}_{210,12}$	210	12	18.69	0	4.91	24	48.15	3600
$\mathcal{M}_{210,14}$	210	14	16.84	0	2.97	28	33.46	3600
$\mathcal{M}_{210,16}$	210	16	13.94	0	2.83	32	31.05	3600
$\mathcal{M}_{210,18}$	210	18	11.35	0	2.26	36	24.87	3600
$\mathcal{M}_{210,20}$	210	20	7.35	0	1.68	40	19.02	3600
$\mathcal{M}_{220,10}$	220	10	23.64	0	6.45	20	70.48	3600
$\mathcal{M}_{220,12}$	220	12	17.4	72	5.12	24	62.01	3600
$\mathcal{M}_{220,14}$	220	14	11.97	0	4.15	28	45.15	3600
$\mathcal{M}_{220,16}$	220	16	11.27	0	3.57	32	33.25	3600
$\mathcal{M}_{220,18}$	220	18	10.45	0	4.32	36	26.01	3600
$\mathcal{M}_{220,20}$	220	20	8.66	0	3.09	40	20.04	3600
$\mathcal{M}_{230,10}$	230	10	24.12	36	6.32	20	80.26	3600
$\mathcal{M}_{230,12}$	230	12	18.07	104	5.86	24	59.45	3600
$\mathcal{M}_{230,14}$	230	14	15.07	0	3.79	28	40.15	3600
$\mathcal{M}_{230,16}$	230	16	14.95	0	4.43	32	34.15	3600
$\mathcal{M}_{230,18}$	230	18	10.61	0	4.37	36	23.45	3600
$\mathcal{M}_{230,20}$	230	20	8.57	0	3.1	40	20.14	3600
$\mathcal{M}_{240,10}$	240	10	28.64	50	6.15	20	99.15	3600
$\mathcal{M}_{240,12}$	240	12	22.05	43	5.57	24	94.02	3600
$\mathcal{M}_{240,14}$	240	14	21.34	0	5.18	28	77.15	3600
$\mathcal{M}_{240,16}$	240	16	17.54	0	3.36	32	45.16	3600
$\mathcal{M}_{240,18}$	240	18	11.15	0	3.54	36	22.35	3600

Table 10: Dimensions of the instances and computational results (cont.)

Case	Size		Resolution					
	$\|\mathcal{F}\|$	$\|\mathcal{L}\|$	z_{ip}	*nodes*	t_{ip}	C-PLEX Calls	z^f_{best}	t^f_{best}
$\mathcal{M}_{240,20}$	240	20	7.02	0	1.76	40	20.35	3600
$\mathcal{M}_{250,10}$	250	10	30.24	234	8.12	20	101.35	3600
$\mathcal{M}_{250,12}$	250	12	24.15	42	8.1	24	80.15	3600
$\mathcal{M}_{250,14}$	250	14	21.45	0	5.12	28	78.11	3600
$\mathcal{M}_{250,16}$	250	16	18.04	0	4	32	64.15	3600
$\mathcal{M}_{250,18}$	250	18	16.41	0	4.26	36	24.48	3600
$\mathcal{M}_{250,20}$	250	20	11.05	0	3.81	40	21.35	3600

References

[1] SESAR Joint Undertaking, European ATM Master Plan, 2nd edition, Technical report (2012).

[2] Joint Planning and Development Office, Next gen air transportation system integrated work plan, Technical report (2008).

[3] EUROCONTROL, Eurocontrol long-term forecast: IFR flight movements 2013–2035, Technical report, Eurocontrol–STATFOR (2013).

[4] T. Lehouillier, J. Omer, F. Soumis, C. Allignol, Interactions between operations and planning in air traffic control, in: Proceedings of the 2nd International Conference of Research in Air Transportation, Istanbul, 2014.

[5] M. Campo, F. Javier, The collision avoidance problem: methods and algorithms, Ph.D. thesis, Universidad Rey Juan Carlos, Madrid (2010).

[6] K. Zhou, J.C. Doyle, K. Glover, et al., Robust and optimal control, Vol. 40, Prentice Hall New Jersey, 1996.

[7] A.U. Raghunathan, V. Gopal, D. Subramanian, L.T. Biegler, T. Samad, Dynamic optimization strategies for three-dimensional conflict resolution of multiple aircraft, Journal of Guidance, Control, and Dynamics 27(4) (2004) 586–594. http://dx.doi.org/10.2514/1.11168

[8] N. Durand, J.-M. Alliot, J. Noailles, Automatic aircraft conflict resolution using genetic algorithms, in: SAC'96 Proceedings of the 1996 ACM Symposium on Applied Computing, Philadelphia, 1996, 289–298. http://dx.doi.org/10.1145/331119.331195

[9] G. Meng, F. Qi, Flight conflict resolution for civil aviation based on ant colony optimization, in: Computational Intelligence and Design (ISCID), 2012 Fifth International Symposium on, Vol. 1, IEEE, 2012, 239–241. http://dx.doi.org/10.1109/iscid.2012.67

[10] A. Alonso-Ayuso, L.F. Escudero, F.J. Martín-Campo, N. Mladenović, A VNS metaheuristic for solving the aircraft conflict detection and resolution problem by performing turn changes, Journal of Global Optimization 63(3) (2015) 583–596. http://dx.doi.org/10.1007/s10898-014-0144-8

[11] R. Vivona, D. Karr, D. Roscoe, Pattern-based genetic algorithm for airborne conflict resolution, in: AIAA Guidance, Navigation and Control Conference and Exhibit, Keystone, Colorado, 2006.

[12] Y. Gao, X. Zhang, X. Guan, Cooperative multi-aircraft conflict resolution based on co-evolution, in: Instrumentation & Measurement, Sensor Network and Automation (IMSNA), 2012 International Symposium on, Vol. 1, IEEE, 2012, 310–313. http://dx.doi.org/10.1109/msna.2012.6324575

[13] N. Durand, J.-M. Alliot, F. Médioni, Neural nets trained by genetic algorithms for collision avoidance, Applied Intelligence 13(3) (2000) 205–213.

[14] M.A. Christodoulou, S.G. Kodaxakis, Automatic commercial aircraft-collision avoidance in free flight: The three-dimensional problem, IEEE Transactions on Intelligent Transportation Systems 7(2) (2006) 242–249. http://dx.doi.org/10.1109/tits.2006.874684

[15] L. Pallottino, E.M. Feron, A. Bicchi, Conflict resolution problems for air traffic management systems solved with mixed integer programming, Intelligent Transportation Systems, IEEE Transactions on 3(1) (2002) 3–11. http://dx.doi.org/10.1109/6979.994791

[16] A. Vela, S. Solak, J.-P. Clarke, W.E. Singhose, E.R. Barnes, E.L. Johnson, Near real-time fuel-optimal en route conflict resolution, IEEE Transactions on Intelligent Transportation Systems 12(1) (2011) 47–57. http://dx.doi.org/10.1109/tits.2010.2051028

[17] M. Christodoulou, C. Costoulakis, Nonlinear mixed integer programming for aircraft collision avoidance in free flight, in: Proceedings of the 12th IEEE Mediterranean Electrotechnical Conference, Vol. 1, IEEE, May 12-15, 2004, Dubrovnik, Croatia, 327–330. http://dx.doi.org/10.1109/melcon.2004.1346858

[18] A. Alonso-Ayuso, L.F. Escudero, F.J. Martin-Campo, Collision avoidance in air traffic management: A mixed-integer linear optimization approach, IEEE Trans. Intell. Transport. Syst. 12(1) (2011) 47–57. http://dx.doi.org/10.1109/tits.2010.2061971

[19] A. Alonso-Ayuso, L.F. Escudero, F.J. Martín-Campo, A mixed 0–1 nonlinear optimization model and algorithmic approach for the collision avoidance in ATM: Velocity changes through a time horizon, Computers & Operations Research 39(12) (2012) 3136–3146. http://dx.doi.org/10.1016/j.cor.2012.03.015

[20] T. Schouwenaars, Safe trajectory planning of autonomous vehicles, Ph.D. thesis, Massachusetts Institute of Technology (2006).

[21] J. Omer, J.-L. Farges, Hybridization of nonlinear and mixed-integer linear programming for aircraft separation with trajectory recovery, IEEE Transactions on Intelligent Transportation Systems 14(3) (2013) 1218–1230. http://dx.doi.org/10.1109/tits.2013.2257758

[22] J. Omer,A space-discretized mixed-integer linear model for air-conflict resolution with speed and heading maneuvers, Computers & Operations Research 58 (2015) 75–86. http://dx.doi.org/10.1016/j.cor.2014.12.012

[23] D. Bertsimas, S.S. Patterson, The air traffic flow management problem with enroute capacities, Operations Research 46(3) (1998) 406–422. http://dx.doi.org/10.1287/trsc.34.3.239.12300

[24] D. Bertsimas, S.S. Patterson, The traffic flow management rerouting problem in air traffic control: A dynamic network flow approach, Transportation Science 34(3) (2000) 239–255. http://dx.doi.org/10.1287/trsc.34.3.239.12300

[25] A.E. Vela, Understanding conflict-resolution taskload: implementing advisory conflict-detection and resolution algorithms in an airspace, Ph.D. thesis, Georgia Institute of Technology (2011).

[26] H.D. Sherali, J. Cole Smith, A.A. Trani, An airspace planning model for selecting flight-plans under workload, safety, and equity considerations, Transportation Science 36(4) (2002) 378–397. http://dx.doi.org/10.1287/trsc.36.4.378.546

[27] S. Resmerita, M. Heymann, G. Meyer, A framework for conflict resolution in air traffic management, in: 42nd IEEE Conference on Decision and Control, Vol. 2, IEEE, December 2003, 2035–2040. http://dx.doi.org/10.1109/cdc.2003.1272914

[28] N. Barnier, P. Brisset, Graph coloring for air traffic flow management, Annals of Operations Research 130(1-4) (2004) 163–178. http://dx.doi.org/10.1023/b:anor.0000032574.01332.98

[29] M. Brochard, Erasmus final report v1.1. Technical report d4.6, EUROCONTROL, Eurocontrol Experimental Centre, Bretigny, France (2009).

[30] R.A. Paielli, Modeling maneuver dynamics in air traffic conflict resolution, Journal of Guidance, Control, and Dynamics 26(3) (2003) 407–415. http://dx.doi.org/10.2514/2.5078

[31] User manual for the Base of Aircraft Data (BADA), Technical report, 11/03/08-08, Eurocontrol (2011).

[32] T. Lehouillier, J. Omer, F. Soumis, G. Desaulniers, A new variant of the minimum-weight maximum-cardinality clique problem to solve conflicts between aircraft, in: H. A. Le Thi, T. Pham Dinh, N. T. Nguyen (Eds.), Modelling, Computation and Optimization in Information Systems and Management Sciences, Vol. 359 of Advances in Intelligent Systems and Computing, Springer International Publishing, 2015, 3–14. http://dx.doi.org/10.1007/978-3-319-18161-5_1

[33] F.A. Administration, Introduction to TCAS II – version 7.1, Technical report, Federal Aviation Administration (2011).

[34] R.M. Karp, Reducibility among combinatorial problems, in: R.E. Miller, J.W. Thatcher, J.D. Bohlinger (Eds.), Complexity of Computer Computations, Springer US, 1972, 85–103. http://dx.doi.org/10.1007/978-1-4684-2001-2_9

[35] I.M. Bomze, M. Budinich, P.M. Pardalos, M. Pelillo, The maximum clique problem, in: D.-Z. Du, P.M. Pardalos (Eds.), Handbook of Combinatorial Optimization, Springer, 1999, 1–74. http://dx.doi.org/10.1007/978-1-4757-3023-4_1

[36] Q. Wu, J.-K. Hao, A review on algorithms for maximum clique problems, European Journal of Operational Research 242(3) (2015) 693–709. http://dx.doi.org/10.1016/j.ejor.2014.09.064

[37] É.D. Taillard, S. Voss, Popmusic — partial optimization metaheuristic under special intensification conditions, in: Operations Research/Computer Science Interfaces Series, Springer Science + Business Media, 2002, 613–629. http://dx.doi.org/10.1007/978-1-4615-1507-4_27

[38] CPLEX v12.5. User's manual for CPLEX, Tech. Rep. 11/03/08-08, IBM ILOG (2014).